A&A 632, A24 (2019)
https://doi.org/10.1051/0004-6361/201936193

Astronomy & Astrophysics

The CARMENES search for exoplanets around M dwarfs

The He I triplet at 10830 Å across the M dwarf sequence*

B. Fuhrmeister[1], S. Czesla[1], L. Hildebrandt[1], E. Nagel[1], J. H. M. M. Schmitt[1], D. Hintz[1], E. N. Johnson[2], J. Sanz-Forcada[3], P. Schöfer[2], S. V. Jeffers[2], J. A. Caballero[3], M. Zechmeister[2], A. Reiners[2], I. Ribas[4,5], P. J. Amado[6], A. Quirrenbach[7], F. F. Bauer[6], V. J. S. Béjar[8,9], M. Cortés-Contreras[3], E. Díez-Alonso[10,11], S. Dreizler[2], D. Galadí-Enríquez[12], E. W. Guenther[13], A. Kaminski[7], M. Kürster[14], M. Lafarga[4,5], and D. Montes[10]

[1] Hamburger Sternwarte, Universität Hamburg, Gojenbergsweg 112, 21029 Hamburg, Germany
e-mail: bfuhrmeister@hs.uni-hamburg.de
[2] Institut für Astrophysik, Friedrich-Hund-Platz 1, 37077 Göttingen, Germany
[3] Centro de Astrobiología (CSIC-INTA), ESAC, Camino Bajo del Castillo s/n, 28692 Villanueva de la Cañada, Madrid, Spain
[4] Institut de Ciències de l'Espai (ICE, CSIC), Campus UAB, c/de Can Magrans s/n, 08193 Bellaterra, Barcelona, Spain
[5] Institut d'Estudis Espacials de Catalunya (IEEC), 08034 Barcelona, Spain
[6] Instituto de Astrofísica de Andalucía (CSIC), Glorieta de la Astronomía s/n, 18008 Granada, Spain
[7] Landessternwarte, Zentrum für Astronomie der Universität Heidelberg, Königstuhl 12, 69117 Heidelberg, Germany
[8] Instituto de Astrofísica de Canarias, c/Vía Láctea s/n, 38205 La Laguna, Tenerife, Spain
[9] Departamento de Astrofísica, Universidad de La Laguna, 38206 Tenerife, Spain
[10] Departamento de Física de la Tierra y Astrofísica & IPARCOS-UCM (Instituto de Fsica de Partículas y del Cosmos de la UCM), Facultad de Ciencias Físicas, Universidad Complutense de Madrid, 28040 Madrid, Spain
[11] Departamento de Explotación y Prospeccón de Minas, Escuela de Minas, Energía y Materiales, Universidad de Oviedo, 33003 Oviedo, Asturias, Spain
[12] Observatorio de Calar Alto, Sierra de los Filabres, 04550 Gérgal, Spain
[13] Thüringer Landessternwarte Tautenburg, Sternwarte 5, 07778 Tautenburg, Germany
[14] Max-Planck-Institut für Astronomie, Königstuhl 17, 69117 Heidelberg, Germany

Received 27 June 2019 / Accepted 3 October 2019

ABSTRACT

The He I infrared (IR) triplet at 10 830 Å is an important activity indicator for the Sun and in solar-type stars, however, it has rarely been studied in relation to M dwarfs to date. In this study, we use the time-averaged spectra of 319 single stars with spectral types ranging from M0.0 V to M9.0 V obtained with the CARMENES high resolution optical and near-infrared spectrograph at Calar Alto to study the properties of the He I IR triplet lines. In quiescence, we find the triplet in absorption with a decrease of the measured pseudo equivalent width (pEW) towards later sub-types. For stars later than M5.0 V, the He I triplet becomes undetectable in our study. This dependence on effective temperature may be related to a change in chromospheric conditions along the M dwarf sequence. When an emission in the triplet is observed, we attribute it to flaring. The absence of emission during quiescence is consistent with line formation by photo-ionisation and recombination, while flare emission may be caused by collisions within dense material. The He I triplet tends to increase in depth according to increasing activity levels, ultimately becoming filled in; however, we do not find a correlation between the pEW(He IR) and X-ray properties. This behaviour may be attributed to the absence of very inactive stars ($L_X/L_{bol} < -5.5$) in our sample or to the complex behaviour with regard to increasing depth and filling in.

Key words. stars: activity – stars: chromospheres – stars: late-type

1. Introduction

Studies of stellar chromospheres typically rely on observations of chromospherically sensitive lines, such as the Ca II H & K lines or the Hα line. In the infrared (IR) regime, the He I IR triplet lines at 10 830 Å are a valuable indicator of chromospheric activity. The He I triplet is formed by transitions from the meta-stable 2^3S level to the 2^3P level, the central wavelengths of the transitions being located at 10 832.057, 10 833.217, and 10 833.306 Å. We note that these and all other wavelengths are given for vacuum conditions since the data used here are measured in vacuum. The latter two components dominate the triplet and remain unresolved in the majority of studies, which is why we refer to the blend of these components as the abbreviation: He I IR line.

The He I triplet lines have frequently been used in solar studies where the lines are strongly modulated by the solar activity cycle (Livingston et al. 2010). They have also extensively been used for chromospheric studies, such as the determination of the magnetic field in solar prominences by spectropolarimetric observations (Orozco Suárez et al. 2014). In the stellar context, the He I IR line has widely been used to study young stars, specifically T Tauri stars, where the triplet is found to be a broad emission component with narrow or broad absorption

* Full Table 2 is only available at the CDS via anonymous ftp to cdsarc.u-strasbg.fr (130.79.128.5) or via http://cdsarc.u-strasbg.fr/viz-bin/cat/J/A+A/632/A24

features. While the emission is thought to originate in the post-shock regions (Dupree et al. 2014), the absorption features serve as a probe of winds and in-falling material around accreting T Tauri stars (Dupree et al. 2005; Edwards et al. 2006), as well as more massive Herbig Ae/Be stars (Cauley & Johns-Krull 2014). Recently, the He I IR triplet has also been found to be a highly informative tracer of the outer atmospheres of exoplanets (e.g., Spake et al. 2018; Nortmann et al. 2018; Salz et al. 2018; Allart et al. 2018; Mansfield et al. 2018; Alonso-Floriano et al. 2019).

Early systematic measurements of the He I triplet lines as a chromospheric indicator in main sequence stars date back to Vaughan & Zirin (1968), who frequently found the triplet lines in absorption for G and K dwarfs. Zirin (1982) extended this study by also identifying the line in some early M dwarf stars. Since then, the line has been extensively used as a chromospheric diagnostic for solar-type stars. For example, Andretta et al. (2017) used the line ratio between He I IR and He I D_3 (at 5877.24 Å) to infer filling factors for active regions of solar-like stars through their comparison to solar models.

The formation scenario of the He I IR triplet lines in the atmospheres of main sequence and giant stars has been under debate for more than 30 yr. The meta-stable ground level of the triplet transitions can be populated by photo-ionisation and recombination (PR) processes, requiring the presence of photons with wavelengths of 504 Å or below to ionise helium. The meta-stable level is then populated by recombining and downward-cascading electrons. Alternatively, in rather dense chromospheric layers, collisional processes can also populate the meta-stable level. To distinguish between these two scenarios, Zarro & Zirin (1986) studied a sample of about 70 dwarfs with spectral types between K3 and F0 and found a correlation between the ratio of X-ray and bolometric surface fluxes, $\log(f_X/f_{bol})$, and the equivalent widths (EW) of the He I line for dwarfs later than (and including) F7, leading Zarro & Zirin (1986) to the conclusion that the PR mechanism makes predictions that are, at least, qualitatively consistent with their observations.

Takeda & Takada-Hidai (2011) observe the He I IR line in a sample of 33 metal-poor late-type stars, of which 24 were dwarfs of type G or hotter, and measure the EWs of the line, EW(He IR), using Gaussian fits. In their dwarf sample, the authors find an EW of 30 mÅ for all low-metallicity dwarfs with [Fe/H] < -1, while stars with higher metallicity demonstrated a larger scatter in their EWs. In combining this data with the findings of Zarro & Zirin (1986), Takeda & Takada-Hidai (2011) find a satisfactory correlation between EW(He IR) and $\log(f_X/f_{bol})$. Smith (2016) studies the work of Zarro & Zirin (1986) which is extended by a number of stars. Like Zarro & Zirin (1986), Smith (2016) finds a satisfactory correlation between He I IR line absorption with fractional X-ray luminosity, L_X/L_{bol}, along with Ca II H&K emission for their later-type sub-sample. However, neither of these samples have included any M dwarfs.

Dupree et al. (2018) study the He I line in a sample of 11 dwarfs with spectral types between G0.5 V and M5 V, observed with the PHOENIX spectrograph mounted at the 4 m Mayall telescope, and find a decrease in EW(He IR) with spectral type for stars later than about K. Further, Dupree et al. (2018) argued that the EW(He IR) is related to the surface X-ray flux for F-through early M-type stars. The latest M dwarf stars in their sample demonstrated the largest surface X-ray fluxes, but only with weak He I IR lines.

While all these correlations between EW(He IR) and X-ray flux can be interpreted in favour of the PR mechanism, they may, alternatively, be caused by a general activity trend. In a theoretical study, Andretta & Jones (1997) showed that there can be a complex interplay between the PR mechanism and collisional excitation. Sanz-Forcada & Dupree (2008) observe active dwarfs, sub-giants, and giants, finding a correlation between EW(He IR) and extreme ultraviolet (EUV) and X-ray fluxes for giants and dwarfs of low activity, but not for the most active dwarfs. These observations indicate that the PR process dominates in giants, while the collisional effects become more relevant in the denser chromospheres of active dwarf and sub-giant stars.

A more detailed picture is obtainable from solar data, where spatially-resolved flare observations by Kobanov et al. (2018) can be interpreted in terms of the PR process. In particular, the He I IR line was strengthened in terms of absorption, while other chromospheric and coronal lines brightened. Nevertheless, the observations showed a time lag with inconclusive interpretation between the emission maximum in the EUV and the absorption maximum in the He I IR line for a second flare maximum. Although many findings favour the PR mechanism, the issue of the appropriate line formation scenario has not been settled.

In M dwarfs, the behaviour of the He I IR line has remained largely unexplored to date. During flares, the He I IR line is observed going into emission along with other helium, Balmer, Paschen, and Bracket lines by, for example, Schmidt et al. (2012), yet detections in absorption remain quite rare since only a few authors include M dwarfs in their studies (Zirin 1982; Dupree et al. 2018) despite the M dwarf sequence exhibiting some major changes in other chromospheric lines. For example, the Hα line emission peaks around M5 V and then declines to an even later spectral type due to the increasing neutrality of these ultra-cool atmospheres (Mohanty & Basri 2003). The question arises, thus, about whether the He I IR line exhibits a similar behaviour.

Here we use a sample of over 300 M dwarfs observed and monitored in the context of the Calar Alto high-Resolution search for M dwarfs with Exo-earths with Near-infrared and optical Echelle Spectrographs (CARMENES) survey to perform a comprehensive study of the He I IR line throughout this spectral type regime. Also using CARMENES data, Schöfer et al. (2019) perform a more general activity study of M dwarfs, including the He I line, but concentrating on other lines and using an entirely different measuring technique. We provide a comparison with this study in Sect. 4.2.

Our paper is structured as follows: in Sect. 2, we give an overview of the data used; in Sect. 3 we describe our pEW measurement method using fits with Voigt profiles and we present our results; a discussion in Sect. 4; and our conclusions in Sect. 5.

2. Observations, sample selection, data reduction, and telluric correction

All spectra used for the present analysis were obtained with CARMENES (Quirrenbach et al. 2018), mounted at the 3.5 m Calar Alto telescope. CARMENES is a two-channel, fibre-fed spectrograph covering the wavelength range from 0.52 to 0.96 μm in the visual channel (VIS) and from 0.96 to 1.71 μm in the near infrared channel (NIR) with spectral resolutions of 94 600 and 80 400 in the VIS and NIR, respectively. The CARMENES consortium is monitoring more than 300 M dwarfs in a comprehensive search for low-mass exoplanets in their habitable zones (Alonso-Floriano et al. 2015; Reiners et al. 2018). To date, CARMENES has obtained more than 14 000

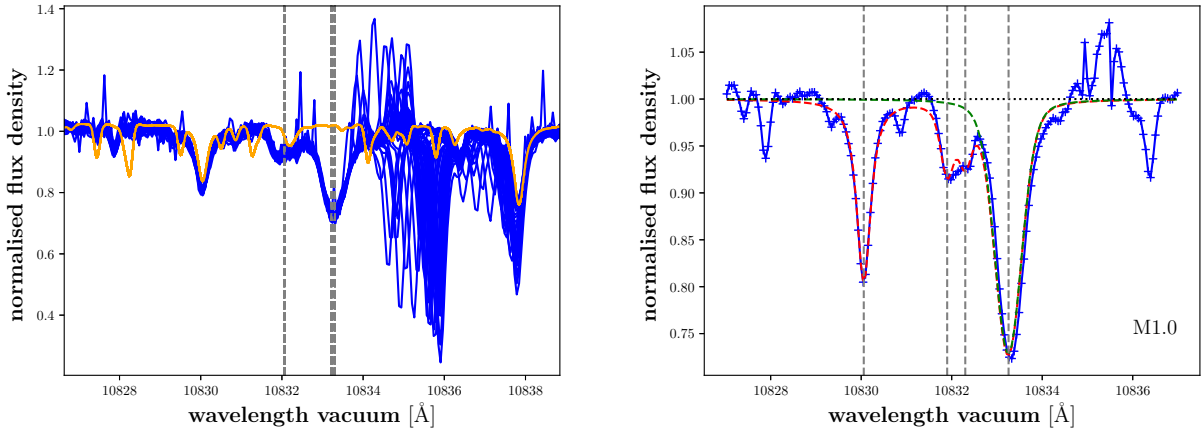

Fig. 1. *Left*: all spectra of J00051+457/GJ 2 used in our analysis in blue. The yellow spectrum is a PHOENIX photospheric model spectrum for comparison. *Right*: co-added and telluric corrected spectrum of J00051+457/GJ 2 in blue with best fit Voigt model in red. The green dashed line represents the He I line component of the fit. At ∼10 835 Å, some artefacts of telluric airglow lines can be seen (shown here in the stellar rest frame). In the left panel, we show the positions of the three components of the He I IR line as dashed grey lines. In the right panel, the grey dashed vertical lines mark the positions of lines considered in the fit (see text for details).

high-resolution visible and near-infrared spectra in the context of this ongoing survey. All spectra are consistently reduced with a dedicated CARMENES reduction pipeline (Zechmeister et al. 2014).

Our study of chromospheric activity visible in the He I IR line is based on the spectra of the 335 stars listed in the CARMENES data archive as of 1 Feb 2019, for which both VIS and NIR spectra are available. After excluding 16 known spectroscopic binaries (Caballero et al. 2016; Baroch et al. 2018), we are left with a sample of 319 M-type stars. This collection of 319 stars is referred to as the whole sample or all sample stars in the following.

As an example of the CARMENES spectra of the He I IR region, we show in Fig. 1 (left panel) the 52 available NIR spectra of the M1.0 V star J00051+457/GJ 2 before telluric correction and normalised around the He I triplet lines. The CARMENES spectral time series are obtained at a temporal cadence optimised for planet detection. Therefore the typical time differences between consecutive observations vary from a day to a few weeks, and only rarely multiple exposures on a given night are available. In the specific case of J00051+457/GJ 2 (shown in Fig. 1), all spectra were taken between July 2016 and December 2017, but for most of our sample stars, there are also more recent spectra. The CARMENES spectral time series are suitable for searches of periodic variations in the chromospheric lines, which we demonstrate in Fuhrmeister et al. (2019). Yet the amplitude of rotational modulation is typically quite low in Hα and Ca II IRT lines, favouring photometric studies to determine rotational periods.

In this respect, the star J00051+457/GJ 2 is a rather typical example of an early M dwarf. As can be seen in Fig. 1, it neither demonstrates strong rotational modulation nor considerable flaring activity in the He I IR line, a result that also holds for other chromospheric lines such as Hα. Although J00051+457/GJ 2 shows Hα in absorption and would therefore formally be classified as inactive, it is not a particularly inactive representative of our sample, which is also indicated by its emission cores in the Ca II H&K lines (Rauscher & Marcy 2006).

As also shown in Fig. 1, many telluric absorption and emission lines are found in the region around the He I IR triplet, with their strengths capable of considerably exceeding the sought-after stellar He I IR line. Furthermore, since the CARMENES spectra are corrected for barycentric velocity shifts, the telluric lines usually pass through the spectra of a given target. The most relevant water absorption lines in the He I IR triplet region (see Rothman et al. 2013; Gordon et al. 2017) are located at 10 829.69, 10 833.32, 10 834.59, 10 835.07, and 10 836.94 Å. To correct for telluric absorption lines, we applied the method described by Nagel et al. (2019) using `molecfit` (Smette et al. 2015; Kausch et al. 2015)[1]. This technique accounts for all water absorption lines in the region, specifically including the ones quoted.

As for airglow lines, upon comparison with the list compiled by Oliva et al. (2015), we identify airglow lines at wavelengths of 10 832.103, 10 832.412, 10 832.271, 110 834.241, and 10 834.338 Å originating in OH; the latter two are not resolved in the CARMENES spectra. To account for the airglow lines, we took particular advantage of the time-variable barycentric shift of the telluric lines with respect to the stellar spectrum. Based on the known wavelengths of the airglow lines, a mask with airglow-affected regions was constructed. Using the Spectrum Radial Velocity AnaLyser (SERVAL) software (Zechmeister et al. 2018), we then co-added the available spectra of each individual star in the barycentric rest frame, substantially down-weighting the masked regions. As a result of this procedure, the impact of the airglow lines is significantly reduced.

The application of the spectral co-addition of the telluric corrected spectra by the SERVAL software produces an averaged spectrum for each star. In Fig. 1 (right panel), we show the resulting averaged spectrum for J00051+457/GJ 2, thus demonstrating our ability to remove the effects of tellurics in our spectra. The averaged spectra are essentially free of telluric absorption lines, althought they may sometimes display artefacts from airglow lines. The quality of the resulting correction for the airglow lines depends, in fact, on the number of available spectra and their distribution in barycentric velocity; for the typical sampling of the CARMENES spectra (Garcia-Piquer et al. 2017), we find that ten spectra are usually sufficient to obtain a satisfactory average spectrum for the star. In the VIS channel of CARMENES, telluric contamination is far less important, especially near the chromospherically active lines relevant to our study, namely, the Hα line, the Ca II infrared-triplet (IRT) lines, and the

[1] https://www.eso.org/sci/software/pipelines/skytools/molecfit

He I D_3 line. In this case, we find that a bin-wise median of the VIS channel spectra yields satisfactory results.

In this paper, we focus on the average spectral properties of our sample. Similar to the case of J00051+457/GJ 2, we verified by visual inspection that, in particular, the earliest M dwarfs in our sample don't show pronounced variability in the He I IR nor in the Hα line. While we, therefore, consider our time-averaged analysis satisfactory in most cases, temporally-resolved analyses are required in individual cases. In the following, we point out cases where variability may have a significant effect on our analysis but we will save a detailed analysis of all time-dependent effects for further discussion in the future.

3. Equivalent width measurements of chromospheric lines

The CARMENES VIS and NIR spectra, averaged as described above and corrected for telluric absorption and emission lines for all 319 M dwarfs form the basis of our study. The spectra of M dwarfs do not show an identifiable continuum because of the ubiquitously present molecular absorption lines; therefore, we employ the method of pseudo equivalent widths (pEWs). The individual steps of our procedure and our results are described in the following sections.

3.1. Photospheric models of the He I IR triplet line region

The strong photospheric background makes any pEW estimation in the region of the He I IR triplet lines challenging. To illustrate the difficulties, we may consider once again the spectrum of the M1 V star J00051+457/GJ 2 (Fig. 1, left panel), where a photospheric model spectrum, computed with PHOENIX (Hauschildt et al. 1999) with an effective temperature of $T_{\rm eff}$ = 3700 K, $\log g$ = 5.0, and solar chemical composition (from the grid by Husser et al. 2013) is overplotted. This most recent PHOENIX spectral library uses local thermal equilibrium (LTE) calculations of atomic and molecular lines in a spherical, one-dimensional geometry. As can be seen from Fig. 1 (left panel), this model reproduces the prominent atomic Si I and Na I lines at 10 830.057 Å and 10 837.814 Å rather well, while other absorption lines are not well reproduced. These lines are likely of molecular origin since, typically, the available molecular line data are far less accurate than atomic line data. Moreover, the observed spectrum of J00051+457/GJ 2 shows a pronounced absorption feature at about 10 833 Å, which is also not reproduced by the model. We identify this feature with the blend of the two reddest and strongest components of the He I IR triplet lines, which do not originate in the photosphere, but rather in the chromosphere. Since PHOENIX calculates only the photospheric emission, but not the chromospheric emission, the feature isn't included in the models. This applies to other chromospheric features as well. Just like the He I IR line, also the He I D_3 and the Hα lines are not present in the PHOENIX photospheric models since they are chromospheric in origin. To a lesser extent, this also holds for the Ca II IRT lines, which demonstrate a much stronger contribution from the photosphere.

3.2. Photospheric lines around 10 830 Å across the M-type regime

In the spectral range from early to late M dwarfs, the photospheric spectrum within which the chromospheric He I IR line is embedded changes considerably, as demonstrated in Fig. 2. For the early M dwarfs, the Si I line at 10 830.057 Å dominates

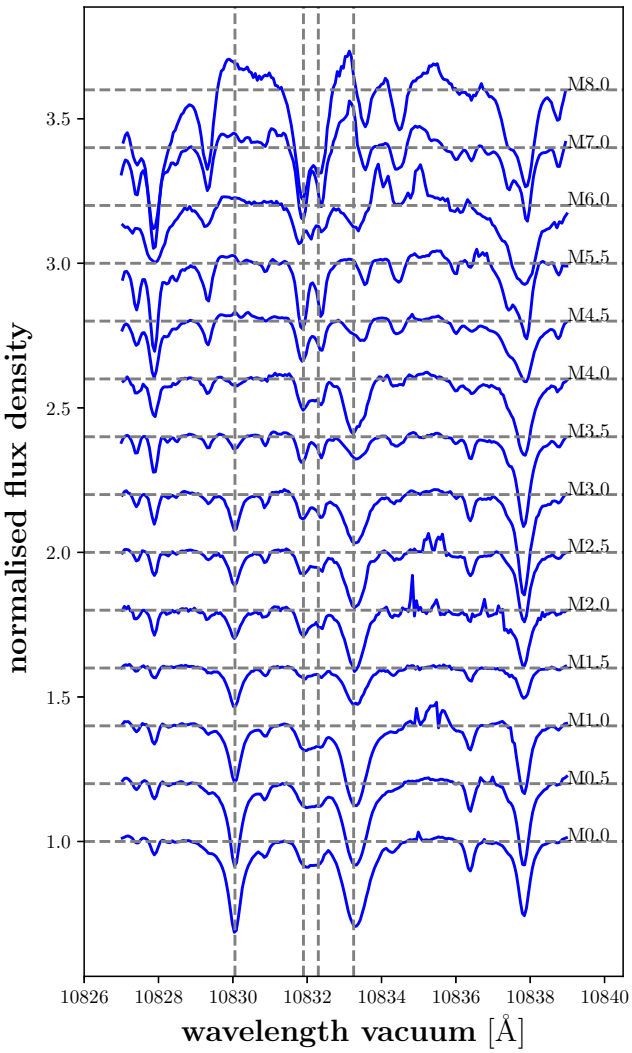

Fig. 2. CARMENES spectra of spectral region around He I IR line across M dwarf spectral sequence exhibiting considerable change from M0 to M8. Each normalised spectrum is offset by 0.2 in flux density for the purposes of clarity. The observed normalised spectrum is denoted in blue with its local pseudo-continuum/offset marked as a dashed grey horizontal line. Vertical grey dashed lines mark the position of the lines considered in the fit. The stars shown are M0.0 V: J03463+262/HD 23453; M0.5 V: J02222+478/BD+47 612; M1.0 V: J00051+457/GJ 2; M1.5 V: J02123+035/BD+02 348; M2.0 V: J01013+613/GJ 47; M2.5 V: J00389+306/Wolf 1056; M3.0 V: J02015+637/G 244-047; M3.5 V: J12479+097/Wolf 437; M4.0 V: J01339-176/LP 768-113; M4.5 V: J01125-169/YZ Cet; M5.5 V: J00067-075/GJ 1002; M6.0 V: J14321+081/LP 560-035; M7.0 V: J02530+168/Teegarden's star; and M8.0 V: J19169+051S/vB10.

the photospheric spectrum, yet this line weakens towards later sub-types and essentially vanishes at a spectral type around M4. The Na I line at 10 837.814 Å starts to deform around that spectral type due to its blending with a line that is, most probably, molecular.

In the wavelength range between these two atomic lines, more spectral features can be seen, which we believe are likely to be molecular in origin, except for the He I line at 10 833.3 Å. Molecular lines gain in strength and number when approaching later spectral types, in contrast to many atomic lines. Moreover, none of these lines is appropriately represented in the PHOENIX model spectrum shown in Fig. 1. This is typically the case for

molecular lines from lesser-known transitions, while atomic data are often known to a much greater extent, as demonstrated by the well-reproduced two atomic lines in the PHOENIX model spectrum. We cannot count out the possibility that unidentified atomic lines also contribute to the spectrum, but we emphasise that the ansatz adopted in our study of the He I IR line does not rely on accurate knowledge of the origin of these lines (see Sect. 3.3).

Between spectral types M3.5 V and M4.5 V, an unidentified line emerges on the red side of the He I line, which becomes stronger towards even later spectral types and is, thus, likely to be of molecular origin. This line can lead to severe blending with the He I IR line, producing triangular shapes for the line, which may complicate the detection and analysis of the He I line. Fortunately, such cases of extreme blending are quite rare. Through visual inspection, we find only seven examples of lines with triangular shapes in our sample, all for stars with spectral types later than M4.0. The molecular line emergence can be seen in more detail in Fig. C.2 from the middle left panel to bottom right panel. The bottom left panel exhibits an example of a triangular line shape for the M6.0 V star J14321+081/LP 560-035. In this case, the fit most likely overestimates the He I IR line strength because of the unresolved blend.

More importantly, the dominance of unidentified lines leads to considerable difficulties in the estimation of the level of the pseudo-continuum for our M dwarfs later than about M5.5 V. To give a better overview of the fit quality across the spectral sequence, we show fits of the He I IR line for the stars used in Fig. 2 and in Figs. C.1 and C.2.

3.3. pEW estimation for the He I IR triplet lines

Since the model spectra do not provide any appropriate reference, we applied the following procedure to measure the pEW of the He I IR triplet lines for the averaged and telluric corrected spectra. First, we fit the spectra in the wavelength range between 10 829 and 10 835 Å with an empirical model consisting of four Voigt profiles to reproduce the pertinent spectral lines in this range; their starting values and free parameters are summarised in Table 1. The component Voigt 1 accounts for the Si I line at 10 830.057 Å, and the component Voigt 4 accounts for the unresolved lines of the He I IR triplet at 10 833.217, and 10 833.306 Å, which are treated as a single line centred at 10 833.25 Å. The components Voigt 2 and Voigt 3 account for the unidentified spectral line components discussed in Sect. 3.2 and they are centred at 10 831.9 Å and 10 832.3 Å. The component Voigt 3 is centred near the weakest component of the He I IR triplet at 10 832.057 Å. However, this triplet component is essentially always blended with the stronger, unidentified feature.

We fit the strengths of all lines and the shape parameters of the component representing the strong Si I line and the two strongest components of the He I IR triplet. The shape parameters of the two components representing the two unidentified features remain fixed because we found this setting most effective in stabilising the fit results considerably. The wavelengths of the components are not varied in our fits. Finally, the pEW of the He I IR line is obtained by integrating the component Voigt 4. Therefore, our pEW values do not refer to the entire triplet. Negative values indicate emission lines, while positive values correspond to absorption lines.

As an example of our procedure, we refer again to the average spectrum of J00051+457/GJ 2 in Fig. 1 (right panel) along with our best-fit model described above. While, admittedly, not all spectral lines in the range can be reproduced reasonably well by our model, the silicon and helium lines are modelled particularly well and, therefore, we consider the chosen approximation sufficient to obtain an accurate estimate of the pEW for the He I IR line.

Table 1. Parameters for Voigt fit.

Parameter	Voigt 1 Si I	Voigt 2 unidentif.	Voigt 3 unidentif.	Voigt 4 He I 2red comp.
Amplitude	−1.0 (free)	−1.0 (free)	−1.0 (free)	−1.0 (free)
Gaussian width σ	0.1 (free)	0.1	0.1	0.1 (free)
Lorentz scale parameter γ	0.1 (free)	0.1	0.1	0.1 (free)
Central wavel. [Å]	10 830.057	10 831.9	10 832.3	10 833.25

Notes. The wavelength span of the whole fit is 10 829–10 835 Å. The continuum is fit by a linear function.

To obtain an error estimate for the pEW, we vary the strength of the best-fit component Voigt 4 and compute the resulting (larger) χ^2 values. Then we fit the resulting χ^2 curve with a second-order polynomial. Finally we determine for which pEW the χ^2 values increases by unity compared to the best-fit value, which yields an estimate of the uncertainty.

3.4. Validity of the pEW estimates for the He I IR lines

Clearly, the fitting procedure described above provides a formal value for the He I IR line strength. However, not all of the derived values are scientifically meaningful. Moreover, the question arises regarding which threshold in pEW(He IR) should be used to decide whether the line is present. Therefore, we visually inspected the averaged spectra for the presence of the He I line and then tried to find criteria to reproduce these findings more objectively. To that end, we first excluded values based on bad fits with a reduced χ^2-value larger than four, and next we discounted insignificant measurements by excluding pEW measurements that were less than 1.5 times the estimated error. The application of these criteria left us with a list of stars with detected He I lines that come quite close to the list of those identified through visual inspection. This procedure should also minimise the number of false detections of the He I line at the expense of more non-detections, where indeed He I lines may be present. The problem of ambiguous spectra cannot be solved totally anyways; also for visual inspection there is a number of mainly late-type M dwarf spectra where presence of the He I line is ambivalent. In the following, we refer to measurements that fulfil both criteria ($\chi^2 < 4$ and pEW(He IR) $> 1.5\ \sigma$) as valid measurements, and the sub-sample of 181 stars for which we derived valid measurements is referred to, accordingly, as a valid sample. Thus, our valid sample comprises 57% of the entire sample of stars and contains detections of the He I IR line with pEW values in the range between −0.27 and 0.75 Å.

As an additional quality check, we inspected all of our spectral fits visually. For most of the early-type M dwarfs, the fit worked quite well (cf., Fig. 1, right panel), whereas for the late spectral sub-types, the fits run into trouble with regard to the pseudo-continuum, and noise artefacts tended to make an

Table 2. pEW measurements of different chromospheric lines for sample stars with valid pEW(He I IR) measurement (full table at CDS).

Karmn	Name	Spec. type [a]	$T_{\rm eff}$ [b] [K]	pEW(He IR) [c] [Å]	σ(pEW(He IR)) [Å]	χ^2	pEW(Hα) [Å]	pEW(Ca IRT) [Å]	pEW(He D_3) [d] [Å]	$L_{\rm X}/L_{\rm bol}$
J00051+457	GJ 2	M1.0	3675	0.247	0.05	0.85	0.352	0.201	−0.051	...
J00183+440	GX And	M1.0	3615	0.118	0.049	0.925	0.324	0.261	−0.047	−4.672
J00286-066	GJ 1012	M4.0	3398	0.076	0.042	2.648	0.138	0.208	−0.043	...
J00389+306	Wolf 1056	M2.5	3537	0.154	0.05	1.33	0.278	0.24	−0.06	−4.771
J00570+450	G 172-030	M3.0	3426	0.117	0.048	2.305	0.139	0.217	−0.059	...
J01013+613	GJ 47	M2.0	3529	0.138	0.049	1.13	0.248	0.238	−0.058	−4.650
J01019+541	G 218-020	M5.0	2900	0.121	0.05	1.014	−5.015	0.038	−0.543	...
J01025+716	BD+70 68	M3.0	3488	0.19	0.05	1.018	0.27	0.23	−0.054	−5.499
J01026+623	BD+61 195	M1.5	3805	0.273	0.05	1.108	0.263	0.177	−0.058	−5.098
J01339-176	LP 768-113	M4.0	3349	0.118	0.046	2.743	−1.611	0.135	−0.174	−3.346

Notes. [a]Taken from Carmencita (Caballero et al. 2016). [b]Taken from Passegger et al. (2018). [c]Positive values of all given pEWs correspond to an absorption line, while negative values correspond to an emission line. [d]Normalisation effects give slightly negative values even for no line present. We use a threshold of pEW(He D_3) < −0.08 Å to accept a measurement as an emission line.

appearance more frequently. We also compared our results to the study by Dupree et al. (2018) whose sample contains four M dwarfs. Two of their objects are also included in our sample, that is, J13536+776/NLTT 35712 and J11054+435/GJ 412A, for which we derive a pEW(He IR) of 0.050 ± 0.050 (which is therefore not among our valid measurements) and 0.112 ± 0.048 Å, respectively. Dupree et al. (2018) reported pEW(He IR) values of 0.067 and 0.139 Å, respectively. Therefore, the derived values and the values found by Dupree et al. (2018) agree within their margins of error. This comparison also suggests that for some stars we may have indeed obtained the correct pEW(He IR) measurements, but which were nonetheless rejected by our conservative selection criteria.

3.5. Overview of the derived pEW(He I IR) estimates

We present all our valid pEW measurements of the He I IR line, the χ^2-values of the Voigt fits, and their errors in Table 2 (full table available from CDS). Besides the CARMENES identification number Karmn (Reiners et al. 2018), we provide the common name, the spectral type of each star as taken from the Carmencita database (Caballero et al. 2016), the effective temperature $T_{\rm eff}$ as taken from Schweitzer et al. (2019), and the $L_{\rm X}/L_{\rm bol}$ values, if known (see Sect. 4.6).

Despite having applied rather conservative He I IR line detection criteria, our sample may still have contained some false positives. In response, we checked for outliers. First, there is only one pEW measurement larger than 0.30 Å, belonging to J01352-072/Barta 161 12. This star demonstrates by far the largest projected rotation velocity ($v \sin i$) in our sample, leading to extreme line broadening (Reiners et al. 2018). The He I IR lines are blended with the neighbouring lines, which leads to the high pEW value. Thus, although the He I line is present in this star, we excluded the star from our sample.

Subsequently, while the majority of the (mean) He I lines in the remaining sample are in absorption, there are ten stars showing the (mean) He I IR line in emission and which fulfil our selection criteria. Looking at both the corresponding averaged spectra and all available individual spectra, we found that in the two cases of J19255+096/LSPM J1925+0938 and J21348+515/Wolf 926, the result can be attributed to noise or telluric artefacts. Consequently, we excluded these stars from our sample as well.

For the remaining eight stars with an average He I IR emission (J02088+494/G 173-039, J05084-210/2M J05082729-2101444, J06574+740/2MASS J06572616+7405265, J10196+198/AD Leo, J11476+002/LP 613-049 A, J12156+526/StKM 2-809, J22518+317/GT Peg, J23548+385/RX J2354.8+3831), we find that the line is variable. Many of these stars belong to moving groups and are associated with the young disc as listed in the Carmencita data (Caballero et al. 2016; Passegger et al. 2019), and they are, therefore, expected to show high levels of activity. In most cases, the He I line region is rather flat in the bona fide quiescent state and the line goes into emission in one or more spectra, which leads to a net emission line in the averaged spectrum. Since the He I excursions are associated with an enhancement in the amplitude of the Hα line, we attribute this to flaring. Moreover, the He I emission tends to be quite broad. Assuming thermal broadening of the He I line for temperatures of about 20 000–25 000 K, we arrive at a Gaussian width of about 0.3–0.4 Å which is consistent with the profiles of the absorption lines. The widths of the emission lines tend to be much greater, which may be caused by such turbulent broadening as is observed during flares (e.g., Linsky et al. 1989; Fuhrmeister et al. 2018). In any case, the emission lines in our sample of averaged spectra are not persistent features. Here, we focus on the averaged spectra and will devote a detailed discussion of the variability of the He I line in a forthcoming paper.

In conclusion, cases where the He I in our averaged spectra is in emission can be explained by individual spectra exhibiting emission caused by flaring or, possibly, the long term variability of these stars. Therefore, we excluded such cases with a negative pEW(He IR) from the valid sample within the discussion of the temperature dependence of the He I IR line strength in Sect. 4.1. We do consider them, however, in our discussion on activity in Sect. 4.5.

3.6. PEW measurements of the He I D_3, Hα, and Ca II IRT lines

In addition to the He I IR triplet lines, we also obtained pEWs of Hα, the bluest line of the Ca II IRT, and the He I D_3 line at 5877 Å. At these wavelengths, telluric contamination plays a minor role, which simplifies the derivation of pEWs considerably. We obtained pEWs for these lines by integrating the median spectrum in specific wavelength intervals. In Table 3,

Table 3. Parameters of EW calculation (all wavelengths in vacuum).

	Centr. wavel. [Å]	Full width [Å]	Reference band 1 [Å]	Reference band 2 [Å]
Hα	6564.62	1.6	6537.43–6547.92	6577.88–6586.37
Ca II	8500.33	0.5	8476.33–8486.33	8552.35–8554.35
He I	5877.24	1.0	5870.00–5874.00	5910.0–5914.0

we list the central wavelengths and full widths of the adopted line integration intervals along with the pseudo-continuum reference bands. We followed Robertson et al. (2016) and Gomes da Silva et al. (2011) in adopting a width w of 1.6 Å for the (full) width of the Hα line band. While the line is normally narrower when seen in absorption, emission lines of slowly to intermediately fast-rotating M dwarfs typically exhibit this width. The line can be much broader in the fastest rotators and during flares (e.g., Linsky et al. 1989; Hawley et al. 2003; Fuhrmeister et al. 2018). While there are only seven stars with $v \sin i > 35$ km s^{-1} in our sample, flaring can be more of a problem for, at least, the most active stars where frequent or vigorous flaring will not average out any further. In those cases, the pEW(Hα) may be underestimated.

For the bluest Ca II IRT line we adopted 0.5 Å for the width of the line band because this line is narrower than the Hα line even when seen in emission. For the He I D_3 line we adopted an intermediate width of 1 Å, which is typical for stars where it is seen in emission. In our analysis, we found no case where the line is clearly seen in absorption. Our pEW estimates for the Hα, the bluest Ca II IRT line, and the He I D_3 line are also listed in Table 2 for the valid sample defined above.

The CARMENES VIS spectra cover even more He I lines, which have been seen as emission lines at least during flares in M dwarfs (Fuhrmeister et al. 2011, 2008). In particular, there is a line at 7065 Å which results from an ortho-helium transition like the He I D_3 and IR lines. Two further lines at 7281 and 6678 Å are caused by para-helium transitions. We screened all averaged spectra for these lines, but we could not identify any of them neither in emission nor absorption. Since the relative intensity of all three lines is lower than that of the He I D_3 line at 5877 Å, these lines may be hidden in the molecular pseudo-continuum; an example is shown in Fig. A.4.

4. Discussion

4.1. Dependence of the He I IR line on effective temperature and spectral type

We first consider the dependence of our pEW(He IR) measurements on the effective temperature $T_{\rm eff}$ and spectral type of the underlying star. In the top panel of Fig. 3, we plot our pEW(He IR) measurements as a function of effective temperature $T_{\rm eff}$, taken from Schweitzer et al. (2019), who also use PHOENIX models for their stellar parameter determination. As can be seen from Fig. 3, the pEW declines towards lower effective temperatures and no valid pEW measurements for the He I line could be derived for the stars with the lowest effective temperatures. Besides, the range of our pEW(He IR) measurements agrees well with corresponding values taken from the literature (Dupree et al. 2018; Andretta et al. 2017; Sanz-Forcada & Dupree 2008), as can be seen in the top panel of Fig. 3. To quantify the relation

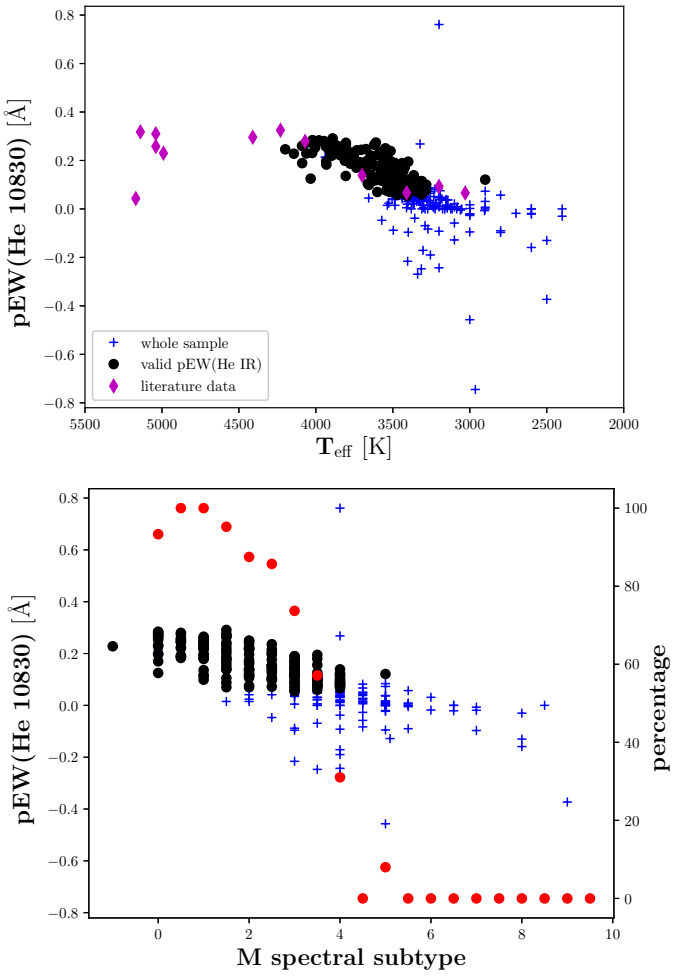

Fig. 3. *Top*: pEW(He IR) as function of effective temperature. *Bottom*: pEW(He IR) as function of spectral type. Blue crosses represent all sample stars (i. e. the non-valid pEWs), while black dots represent the as valid selected pEWs. In the *top panel*, magenta diamonds represent literature data from Sanz-Forcada & Dupree (2008), Andretta et al. (2017), and Dupree et al. (2018). In the *bottom panel*, red dots correspond to the right y-axis and give the percentage of valid measurements for the selection criteria, (see text).

between effective temperature and pEW(He IR), we computed Pearson's correlation coefficient using all valid measurements of absorption lines, which yields a correlation coefficient of 0.75 with a p-value of 2.7×10^{-32}. Thus, we conclude that pEW(He IR) does depend on effective temperature.

Not surprisingly, a similar behaviour is identified when plotting the pEW(He IR) measurements as a function of spectral type instead of effective temperature, as can be seen Fig. 3, bottom panel. There we also provide the detection fraction as a function of spectral type. No valid detections were made for stars later than M5, whereas for the earlier M dwarfs, the valid detection rates approach 80%. More specifically, among the very earliest M dwarfs, the detection fraction of the He I line is close to 100%, and there is only one M0.0 V and one M1.5 V star (J04219+213/LP 415-17 and J15218+209/OT Ser, respectively), where we failed to detect the He IR line. Visual inspection of the spectrum of J04219+213/LP 415-17 suggests that the non-detection of the He I line is actually caused by noise artefacts, while the spectrum of the young active star OT Ser displays only a shallow absorption line. This star is the only one of its

spectral sub-type exhibiting Hα in emission and shows at least two flares in the CARMENES time series. Not surprisingly, also the individual spectra of the He I lines show variability, including absorption and emission in the He I line. We therefore argue that in the case of OT Ser the He I line is actually filled in in the averaged spectrum of this star, which hindered its formal detection.

Beyond the spectral sub-type M1.5 V, the detection fraction of the He I line decreases systematically. For sub-types M2.0 V and M2.5 V, six stars have non-detections of the He I line, and two of them show artefacts of telluric airglow lines in the averaged spectrum that misled the fit. Another two stars seem to show very shallow absorption lines, which are considered invalid by our automatic selection procedure. The two remaining stars have quite flat spectra in the region of the He I line. The latter four stars are among the least active in the groups pertaining to their spectral sub-type as measured by the pEW(Ca II IRT) and they show also no sign of activity in their Hα lines. Therefore, we argue that the He I line is not filled in, but is most likely to be intrinsically weaker than in the other stars of this spectral type.

At spectral type M4.0–M4.5 V, the detection fraction has significantly declined. Out of the 75 sample stars in this spectral type regime, we end with only 18 valid pEW(He IR) measurements. The 57 stars without valid pEW(He IR) measurements span the whole range of activity levels seen in stars with this spectral sub-types. Scrutinising the spectra of these stars with high activity levels as indicated by low pEW(Ca IRT) values, we find that they are affected by variability, which effectively acts as a fill-in in the average spectra. These active stars may have a detectable He I line during pure quiescent states (which we do not see because of averaging in the flaring phases as identified by looking at the variability in the Hα emission). In contrast, the spectra of the inactive stars really have shallow or flat He I lines.

Turning now to even later sub-types, among the 23 M5.0 V stars in our sample, a valid measurement of the pEW(He IR) could only be obtained for the star J01019+541/G 218-020. This star is a fast rotator with $v \sin(i) = 30$ km s^{-1} measured by Reiners et al. (2018) and could be associated with the Ursa Majoris moving group (Caballero et al. 2016). The remaining 22 M5.0 V sample stars with He I non-detections have a wide range of rotation periods and Hα activity levels with the majority showing Hα in emission. A contribution of the He I line is revealed by its variability for many of these stars when looking at the individual spectra. Since we have only snapshots rather than continuous observations it is hard to identify the reasons for temporal activity variations in these stars. The Hα line can reveal obvious flaring, but may remain inconclusive when observed in the late decay phases of flares, when it may have returned to quiescent levels while other chromospheric lines are still in emission. Although periodic modulation by rotation or even cycles may contribute to the variability in chromospheric lines, we consider flaring to be the most probable explanation for the mid M dwarfs, because it is a phenomenon frequently observed for such objects.

Nonetheless, it appears that the He I line is weak or absent during the most inactive phases of these late M stars. These findings are consistent with a weakening of the line towards later spectral types and a resulting decline in the detection fraction.

The vast majority of the M-type sample stars later than M4.0 V shows Hα in emission, demonstrating the existence of chromospheres (and presumably coronae) in these objects. This might suggest a general filling in of the line as an explanation for the observed weakening of the line towards later spectral types. However, we argue against this hypothesis as follows: we do not observe the He I IR line going into emission during the quiescent state, which is what we would expect to happen had there been any activity-driven fill-in for the line. We consider it unlikely that the He I line is fully filled in, but it is neither visible in absorption nor in emission during the quiescent state. However, it appears that the line can easily be observed in emission during flares, when EUV fluxes are enhanced. Moreover, the densities are likely to be much higher and, therefore, collisions may also contribute significantly to the line emission. Another explanation for the observation of an emission line is that the emitting material may be located off-limb, dominating the line flux.

Therefore, it appears likely that for stars later than about M4, the conditions for the formation of the He I line are different in comparison to those for stars of an earlier type. This refers to the upper chromosphere and lower transition region, where the He I line is expected to originate (in the case of the photo-ionisation and recombination process, the line is formed in the upper chromosphere, while collisional processes are expected to take place in the lower transition region for temperatures exceeding 20 000 K, see Andretta & Jones 1997). Possible changes inhibiting the formation of the He I line encompass: (*i*) a lower density in the chromosphere so that fewer atoms can interact with the photospheric light (but, in contrast, the Hα emission in those stars demonstrate relative high densities), (*ii*) a lower EUV radiation level, which leads to less He I ionisation and therefore fewer recombinations to the meta-stable lower level of the He I IR line (although high levels of X-ray radiation persist for later spectral type stars in our sample, see Sect. 4.6), (*iii*) a reduced geometrical thickness of the layer where the He I line is formed. The latter possibility was demonstrated in simulations based on solar chromospheric models by Avrett et al. (1994) which resulted in a reduced He I line absorption for the same coronal illumination and chromospheric densities.

Finally, the steep decrease in the detection fraction of the He I IR line takes place at those spectral types where M dwarfs ought to become fully convective, which is believed to happen around M3.5. However, this concurrence might be coincidental and, thus, proof of a physical link between these two phenomena remains elusive at this moment.

4.2. Comparison to previous studies of the He I IR line

Schöfer et al. (2019) have also recently used the CARMENES sample of spectra to study chromospheric activity in various spectral lines. Schöfer et al. (2019) use the spectral subtraction technique, which relies on subtracting the spectrum of an inactive reference star before any pEW measurement. This technique is especially efficient for chromospheric lines that have a photospheric contribution to be subtracted out, which is not the case for the He I IR line. For each spectral sub-type, Schöfer et al. (2019) use the spectrum of the star with the longest (known) rotation period as a reference. Therefore, these results are effectively "differential pEW" measurements that are defined with respect to the chosen reference star.

Schöfer et al. (2019) find that the differential pEW is about just as often negative as positive for early M0–1 V spectral types, with excess absorption occurring more often in M1.5–4.0 V type stars with respect to the template. Therefore Schöfer et al. (2019) also measure some variation of their differential pEW(He IR) with spectral type. Their results are, nevertheless, not easily compared to ours because the dependence on spectral type is eliminated by the application of the spectral subtraction of the reference star.

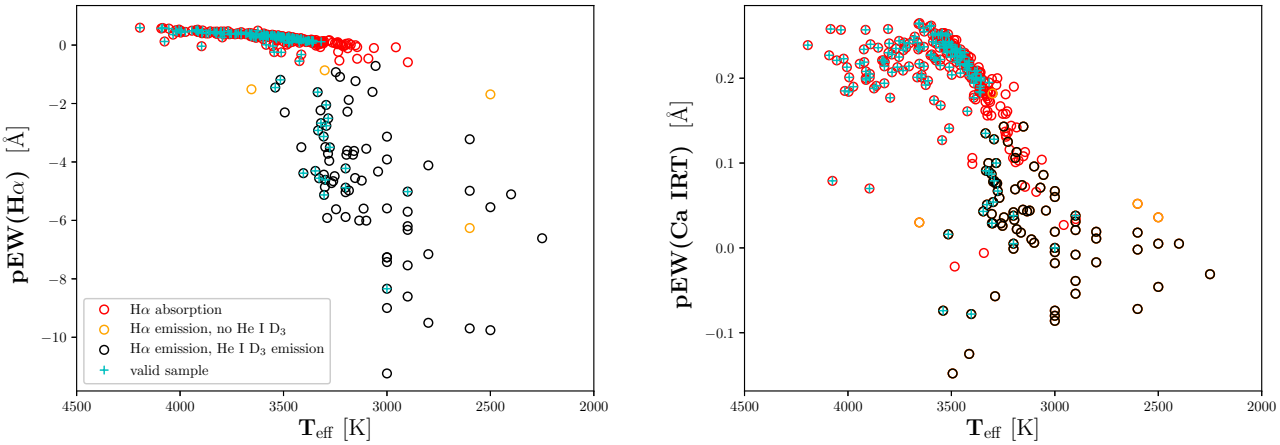

Fig. 4. Relation between stellar effective temperature and pEW for the chromospheric Hα (*left*) and Ca II IRT lines (*right*). Cyan crosses represent the valid sample as defined for the He I IR line measurements. Red circles represent stars with Hα in absorption. Black circles represent stars with both the Hα and the He I D_3 line in emission, and orange circles symbolise stars with spectra showing only Hα in emission.

The He I triplet has also been studied by Sanz-Forcada & Dupree (2008), Andretta et al. (2017), and Dupree et al. (2018). In the upper panel of Fig. 3, we additionally plot their measurements of the pEW(He IR) for twelve stars later than K0 (magenta diamonds). Since these papers state spectral type or $B-V$ colour but no effective temperature, we made our conversions into temperature based on the relations provided by Mamajek et al. (2013). There are seven stars with effective temperatures below 4500 K and, as shown in Fig. 3, despite their low number, these complementary measurements show the same decrease in pEW(He IR) towards lower effective temperature.

Moreover, these additional data suggest the existence of a "saturation regime" for He I line absorption at a pEW of about 300 mÅ, which appears to have been reached for the earliest M dwarfs, and extends towards higher effective temperatures. Our largest pEW measurements are just below 0.3 Å, which is well below the limit of 0.4 Å for single active dwarfs, which Andretta & Giampapa (1995) derived theoretically based on model calculations for solar-type stars.

4.3. Dependence of Hα and Ca II IRT on effective temperature

In Fig. 4 we show the dependence of the pEW measured for the Hα and Ca II IRT lines on photospheric temperature. Since measuring pEW(Hα) and pEW(Ca IRT) in all sample stars is straightforward, we show our measurements for the whole stellar sample. The valid sample in terms of meaningful He I IR line measurements is indicated by cyan crosses. We further indicate whether Hα is seen in absorption (red circles) or emission (black circles). For most stars, Hα seen in emission goes along with He I D_3 seen in emission, and those stars where Hα is seen in emission without He I D_3 are indicated by the orange circles.

The measured value of pEW(Hα) is frequently used to formally differentiate between active stars with Hα in emission and inactive stars. However, the actual pEW(Hα) threshold below which an Hα line is considered to be a true emission line has varied between different authors: Jeffers et al. (2018) adopt −0.5 Å; West et al. (2011) −0.75 Å; and Newton et al. (2017) −1.0 Å. Here have applied a threshold of −0.6 Å for the pEW(Hα) value to mark the active stars in Fig. 4.

Based on this criterion, all active stars in our sample have effective temperatures cooler than about 3500 K, and with the exception of two stars, all sample stars below 3000 K show Hα in emission. The pEW(Hα) values of these active Hα emitters form a widely spread-out cloud. Nevertheless, there is a loose correlation between their pEW(Hα) and effective temperature with a Pearson r-value of 0.5 and a p-value of 1.8×10^{-6}. For the inactive dwarfs with Hα seen in absorption there is a rather tight relation, such that the pEW(Hα) values decrease towards cooler stars, a result also found by Stauffer & Hartmann (1986), Newton et al. (2017), and Jeffers et al. (2018).

A similar behaviour is seen for the Ca II IRT line. For stars with Hα in emission, the pEW(Ca IRT) values also show large scatter. For the more inactive stars, the pEW(Ca IRT) declines with cooler effective temperature, which is most clearly seen for stars with effective temperatures between about 3800 K and 2800 K. The Ca II IRT line goes into emission only for the most active stars.

4.4. Relation between the He I IR line and the Hα and Ca II IRT lines

We next turn to the relation between pEW(Hα) and pEW(He IR) for individual spectral sub-types shown in Fig. 5. We note that only stars with valid measurements of pEW(He IR) are considered here. The left panel shows the early spectral sub-types, while the right panel shows the late sub-types. The figure indicates that the Hα active stars demonstrate a correlation of pEW(He IR) to pEW(Hα), while the inactive stars are grouped in a tight band. Looking at the left panel, for sub-types earlier than about M3 for the inactive stars, a nearly vertical band can be noted for each sub-type. When looking specifically at M1.0 V stars, higher values of pEW(He IR) are shown to correspond to higher values of pEW(Hα). This implies that both lines become deeper absorption lines until a maximum value is reached. Then the trend reverses and both lines start to fill in and finally go into emission (only for sub-types later than or equal to M2 is Hα emission observed). In summary, for increasing levels of activity for inactive stars both the Hα and the He I IR line become deeper absorption lines until a certain (sub-type dependent) value is reached, when both lines start to become more shallow again, that is, they fill in.

For spectral sub-type M4, it appears that pEW(Hα) decreases for increasing pEW(He IR), indicating that the Hα line has already started to fill in for the inactive stars. For spectral

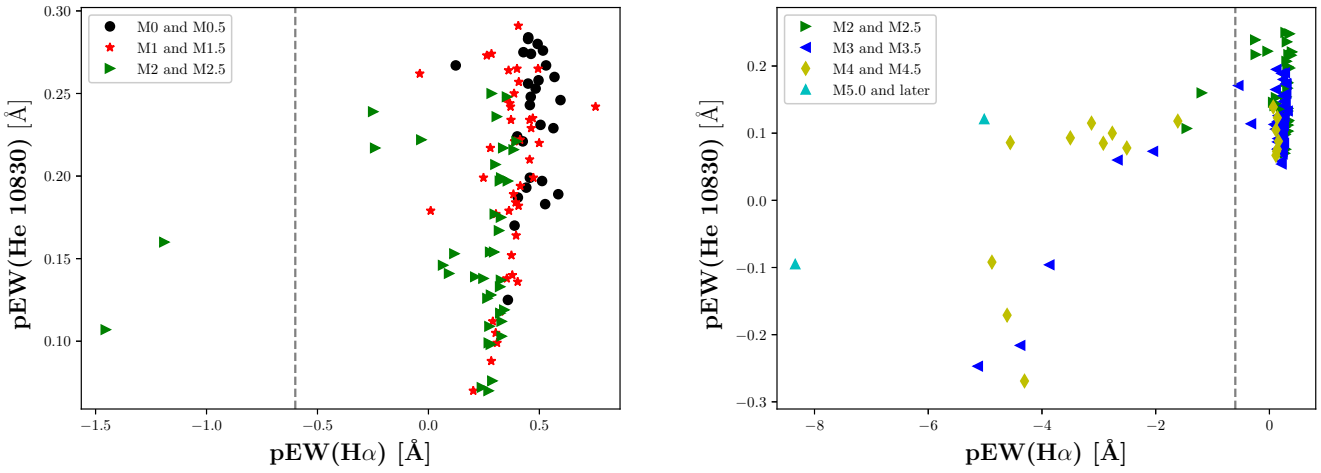

Fig. 5. Valid measurements of pEW(He IR) as function of pEW(Hα) for different spectral types as given in legend. The dashed vertical line marks the dividing line between active (Hα in emission) and inactive stars (Hα in absorption) for both panels. The cloud of inactive late-type M dwarfs (*right*) connects smoothly to the cloud of the inactive early-type M dwarfs (*left*) shifting to lower maximum values for later spectral types. For better comparison, we show spectral type M2/M2.5 in both panels.

sub-types M5 V and later, there are no inactive stars in the sample. Generally, for the active stars, the He I IR line appears to show a decrease in pEW for decreasing pEW(Hα), indicating an increasing activity level. However, filling in does not appear to occur in quiescence, but it is, rather, associated with flares or, at least, episodes of enhanced activity. Particularly when it comes to the spectral sub-types M4 and later, the picture in Fig. 5 is likely dominated by flares for the lowest values of both pEW(Hα) and pEW(He IR). This is in line with increasing flare duty cycles from 0.02% for early M dwarfs to 3% for late M dwarfs found by Hilton et al. (2010). In fact, visual inspection suggests that all sample stars with Hα in emission (pEW(Hα) < −0.6 Å) show changing levels of activity during observation, which do not average out and, therefore, "contaminate" the pEWs to some extent. However, in contrast to the He I IR line, the Hα and Ca II IRT (and also the He I D_3 line) can turn into emission lines not only for flares, but also during the quiescent state.

The Ca II IRT lines are also frequently used as activity indicators (Mittag et al. 2017; Martin et al. 2017). In Fig. 6 we show the analogous relation between pEW(Ca IRT) and pEW(He IR). Since the Ca II IRT line only fills in for higher levels of activity, the relation between the two quantities in the low-activity regime is more pronounced when compared to the case of pEW(Hα).

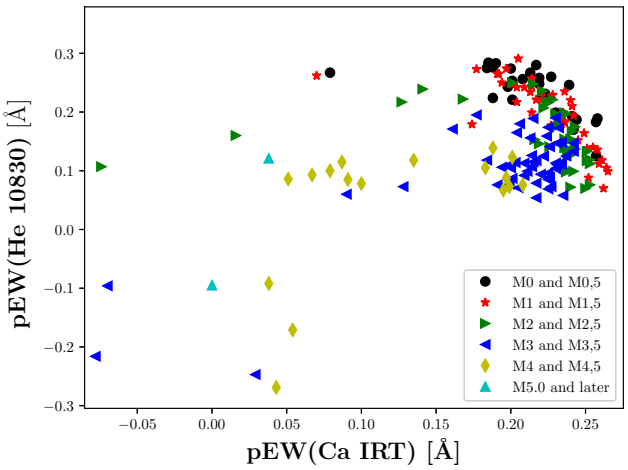

Fig. 6. Valid pEWs of He I IR line as function of pEW(Ca IRT) for different spectral types as given in legend.

4.5. Relation between the He I D_3 and IR lines

Since the lower level of the He I D_3 line is the upper level of the He I IR line, simultaneous measurements of both lines can provide additional diagnostics. This is the method used, for example, by Andretta et al. (2017) to infer filling factors for active regions of solar-like stars by comparison to solar chromospheric models. In Fig. 7, we show the relation between the measured pEWs for the He I D_3 line at 5877 Å and the He I IR line. Among the inactive stars in our sample, we neither detect the He I D_3 line in absorption nor emission. The measurements by Andretta et al. (2017) suggest that the He I D_3 line is very weak and, therefore, difficult to detect on top of the molecular pseudo-continuum of our stars (see Fig. A.3). Moreover, due to normalisation effects, we measured a slightly negative pEW(He D_3) for inactive stars (see Fig. 7). Therefore, we opted for a threshold of pEW(He D_3) < −0.08 Å for the acceptance of a measurement as an emission line. For the 24 stars for which a non-zero value for pEW(He D_3) could be measured, it is correlated to pEW(He IR). Moreover, pEW(He D_3) is tightly correlated with pEW(Hα). Consequently, these active stars show a spectral type-dependent correlation, which is almost identical to that seen for the Hα line.

In stars where the He I D_3 line is seen in emission, the He I IR line can be in absorption (13 stars) or in emission (7 stars). For the latter seven stars, all show $L_X/L_{bol} > -3.5$ and effective temperatures below 3550 K. Furthermore, for all sample stars with the He I D_3 line in emission and the He I IR line detected, Hα is also in emission. Visual inspection reveals that all of these stars undergo temporary enhancements in their Hα emission, which we attribute to flaring activity. The He I IR line is, therefore, also affected by flaring, and more severely or more often for the stars where it is seen in emission. The He I IR line is observed during the quiescent state as an absorption line or not observed at all in these stars. By contrast, the He I D_3 line can also be observed in emission during the quiescent state.

Unlike the He I IR line, the He I D_3 line tends to go into emission for late spectral types, which we interpret as a (quasi-)

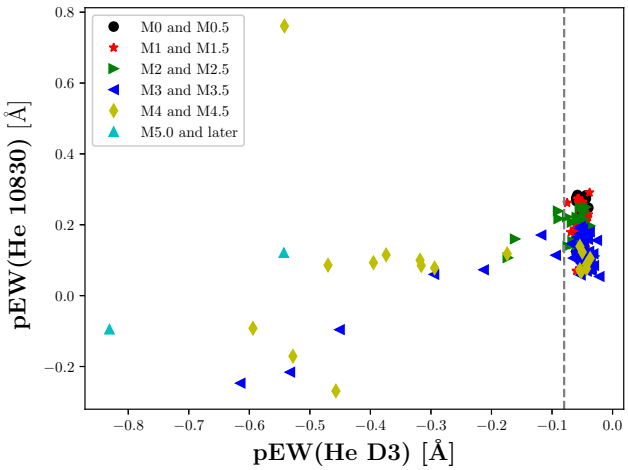

Fig. 7. Valid (according to our selection criterion) pEW(He IR) as function of pEW(He I D_3) for different spectral types given in legend. The grey dashed vertical line indicates the threshold for the line in emission for lower values or non-existent for larger values.

continuum effect. PHOENIX spectra demonstrate that for mid M dwarfs the continuum around the He I D_3 is a factor of 100 lower than at the wavelength of the He I IR line, while it is comparable for M0 stars. A detection of the He I D_3 line against the weak background in late-type M dwarfs is, therefore, less challenging than in early-type stars. If the line is truly absent in the inactive dwarfs or is merely undetectable, remains unknown. Yet it seems that a minimum level of activity is needed to drive the line into notable emission, and this level coincides with the parameter beyond which Hα goes into emission as well.

Andretta et al. (2017) also found a correlation between the He I D_3 and the He I IR lines for earlier-type stars. However, the authors find He I D_3 in absorption, which we never observe for the CARMENES M dwarfs, and they derive a positive correlation between pEW(He IR) and pEW(He D_3), measuring values from 0.003 to 0.07 Å for the latter. Our study is not sensitive enough to measure such small pEWs in the presence of the surrounding photospheric molecular lines. The sample of Andretta et al. (2017) reaches down to a spectral type of about K3, so that there is a gap between the coolest stars in their sample and the hottest ones in our sample. Their latest-type stars show the lowest pEW(He D_3) values, which is consistent with our results. Houdebine et al. (2009) use a spectral subtraction technique to study the He I D_3 line in 37 M1 stars and find measurable absorption for one M1 dwarf (Hα in absorption) and eight M1e dwarfs (Hα in emission), but they do not find emission (just as we also found no emission) in these early M dwarfs. The stars with the strongest absorption in their sample are, unfortunately, not included in our sample.

4.6. Relation between chromospheric helium lines and X-ray emission

Several authors, such as Zarro & Zirin (1986), Takeda & Takada-Hidai (2011), and Smith (2016), have reported a correlation between the EW of the He I IR line and the X-ray luminosity (L_X) scaled by the bolometric luminosity (L_{bol}) for stars of spectral type K and earlier, and argue that this finding is in line with the photo-ionisation and recombination mechanism: if more soft X-ray and EUV photons are present to ionise helium, more electrons eventually end up in the meta-stable $^3S_1$ ground state of the He I IR triplet lines, which then carry out more absorptions that cause a deeper absorption line. While Sanz-Forcada & Dupree (2008) find no correlation between X-ray flux and pEW(He IR) for highly active earlier-type dwarfs, they do find it for giants and low-activity dwarfs. They attribute this discrepancy to different levels of population mechanisms. In the thinner atmospheres of giants, the photo-ionisation and recombination mechanism dominates, while collisions may prove more significant in the far denser dwarf atmospheres.

In Fig. 8, we show the distributions of pEW(He IR) as a function of $\log(L_X)$ in the left panel and of $\log(L_X/L_{bol})$ in the right panel for our sample stars. The L_X values were derived from X-ray fluxes given in the Carmencita database (Caballero et al. 2016), which were measured mainly within the ROSAT all-sky survey in the 0.1–2.4 keV energy band (Voges et al. 1999). For 154 stars, we actually obtain L_X detections and upper limits on the X-ray flux for the remaining stars based on the ROSAT survey, but we find that including ROSAT upper limits does not contribute any significant information relevant to the analysis carried out here. The resulting $\log(L_X/L_{bol})$ values range from −5.7 to −2.2 for the stars in our sample, while $\log(L_X)$ values range from 26.1 to nearly 30.0. A number of stars in our sample exhibit $\log(L_X/L_{bol})$ values in excess of the saturation limit of about −3 (see, e. g. Pizzolato et al. 2003), suggesting that X-ray flaring probably affected the measurement, especially in the most extreme cases. For reference, we also show the L_X/L_{bol} values as a function of effective temperature in Fig. B.1. Obviously, none of these X-ray measurements have been carried out simultaneously to our CARMENES data. As a result, this procedure may lead to comparisons between measurements at different activity levels, in particular, flaring X-ray luminosity and quiescent pEW(He IR) values may be compared or vice versa.

In the following, we focus on stars whose measurements are unaffected by flaring, namely, those for which we obtained $\log(L_X/L_{bol}) < -3$ and absorption in the He I IR line, that is, a positive value for pEW(He IR). Here we note that the population of the diagram at the low X-ray luminosity end is limited by the sensitivity of X-ray measurements. In particular, there is a lack of stars with measurements of $\log(L_X/L_{bol}) < -5.5$ which support the relation in the study by Sanz-Forcada & Dupree (2008) or Zarro & Zirin (1986). In Fig. 8, we indicate estimates for the lower and upper envelopes of the distribution for each spectral sub-type. Neither distribution shown in Fig. 8 shows a clear correlation between pEW(He IR) and X-ray properties. What the diagram does show is that for comparatively low activity levels of $\log(L_X/L_{bol}) = -5$, the whole range of pEW(He IR) can be observed. This is particularly pronounced for the M1 V spectral types. For the early types M0 V and M1 V, the distributions further suggest a dividing line indicating that low values of pEW(He IR) are not observed at high activity levels. This part of the diagram is more complete in the sense that the majority of active early type stars have X-ray detections. For the spectral types later than M3.0 V, the tendency cannot be discerned and He I IR and X-ray properties appear essentially uncorrelated.

The He I IR line is only seen in emission in stars which are also very active by X-ray standards ($\log(L_X/L_{bol}) \geq 3.5$). There is a tendency for more X-ray luminous stars to also show stronger emission in the helium line. The same is true for the He I D_3 line. We find a correlation between pEW(He D_3) and $\log(L_X/L_{bol})$ for these active stars with a Pearson correlation coefficient of −0.44 and a p-value of 1.5×10^{-5}. Similarly, the Pearson correlation coefficient between pEW(He IR) and $\log(L_X/L_{bol})$ is −0.24 with a p-value of 0.02. Therefore, stronger X-ray emission tends to be associated with stronger emission in the helium

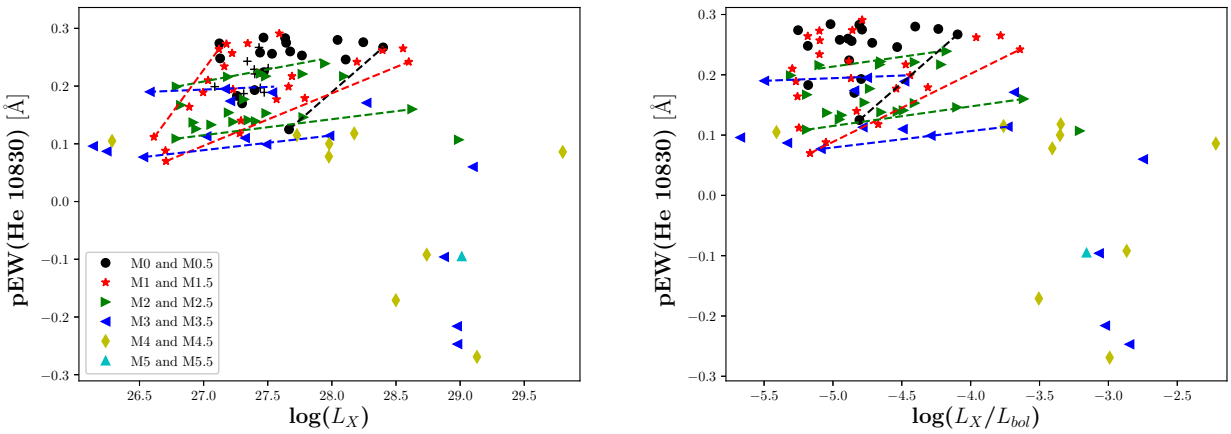

Fig. 8. Measurement of pEW of He I IR as function of L_X (*left panel*) and of L_X/L_{bol} (*right panel*). Symbols represent the pEW(He IR) of the valid sample with known X-ray fluxes, and colours decode spectral sub-type as in the legend in the left panel. In both panels, dashed lines with colours according to sub-type indicate hypothesise lower and upper envelopes where recognisable, while for the other spectral sub-types only lower envelopes are indicated.

lines. However, the measurements may be affected by X-ray flaring in this regime, especially in the most extreme cases, and we believe that this is also the case for the measurement of the helium lines. This is consistent with these stars also acting as highly active Hα emitters. Any correlation in this high-activity regime is, therefore, probably affected by flaring.

5. Summary and conclusions

We present a comprehensive study of the He I IR line in the co-added CARMENES spectra of a sample of 319 M dwarfs ranging from M0.0 V to M9.0 V with various levels of activity. Since the surroundings of the He I line contain a number of unidentified spectral features, which are not satisfactorily reproduced by synthetic spectra covering the range of M-type stars, we model the immediate spectral environment of the He I IR line using an empirical model consisting of four Voigt components, which provides adequate pseudo equivalent widths of the line. Upon applying a conservative approach, we obtained 181 valid measurements in our sample of 319 stars. The detection rate of the He I IR line strongly depends on spectral sub-type. Our results are consistent with the hypothesis that the He I line is always present in the earliest-type M dwarfs, while the detection fraction continuously decreases with spectral sub-type and, for stars later than about M5, the He I line is not detectable.

The observed strength of the He I IR line depends on the effective temperature of the star. In particular, it is strongest in early-type M dwarfs where we find maximum pEW values of around 300 mÅ. The absorption strength of the line declines towards later spectral types. The line is usually seen in absorption with a few exceptions, which we attribute to flaring activity. At least in these latter cases, the He I IR line can exhibit prominent temporal variability, a detailed discussion of which is beyond the scope of this paper. In contrast, the He I D_3 line is undetectable in the spectra of inactive stars, while it is seen in emission in active stars regardless of spectral sub-type. We could not establish the presence of any other He I line in the CARMENES spectral range in our averaged spectra.

We interpret the observed decline in pEW(He IR) with effective temperature in inactive stars without a detectable continuation into emission as evidence for a true, physical disappearance of the line as opposed to an increasing level of fill-in caused, for example, by collisional excitation. If the line were collisionally controlled, rising activity levels would be expected to raise the population of the upper level, entailing first a fill-in in the line before driving it into emission. However, in our sample the weakest observed He I IR line absorption seems to correspond to the most inactive stars as measured by Ca II IRT for the sub-types earlier than about M3.0 V.

We studied the relation between pEW(He IR) and the stellar X-ray properties. No clear correlation between the He I IR absorption and the X-ray emission is observed. Our data show that the maximal level of He I IR absorption can already be reached at low activity levels of $\log(L_X/L_{bol}) = -5$. Moreover, we find no early-type M dwarfs in our sample that would show weak absorption in the He I IR line at high activity levels. Emission in the He I IR line is only observed during flares in our sample.

Our results are consistent with the role of photo-ionisation and recombination mechanism as the main driver of He I IR line formation. Although we do not detect the line in stars later than M5 V, our study shows that the He I IR triplet lines are a ubiquitous feature in earlier-type M dwarfs, which carries great diagnostic weight for future chromospheric structure and activity studies.

Acknowledgements. B.F. acknowledges funding by the DFG under Schm 1032/69-1. CARMENES is an instrument for the Centro Astronómico Hispano-Alemán de Calar Alto (CAHA, Almería, Spain). CARMENES is funded by the German Max-Planck-Gesellschaft (MPG), the Spanish Consejo Superior de Investigaciones Científicas (CSIC), the European Union through FEDER/ERF FICTS-2011-02 funds, and the members of the CARMENES Consortium (Max-Planck-Institut für Astronomie, Instituto de Astrofísica de Andalucía, Landessternwarte Königstuhl, Institut de Ciències de l'Espai, Institut für Astrophysik Göttingen, Universidad Complutense de Madrid, Thüringer Landessternwarte Tautenburg, Instituto de Astrofísica de Canarias, Hamburger Sternwarte, Centro de Astrobiología and Centro Astronómico Hispano-Alemán), with additional contributions by the Spanish Ministry of Economy, the German Science Foundation through the Major Research Instrumentation Programme and DFG Research Unit FOR2544 "Blue Planets around Red Stars", the Klaus Tschira Stiftung, the states of Baden-Württemberg and Niedersachsen, and by the Junta de Andalucía. Based on data from the CARMENES data archive at CAB (INTA-CSIC). We acknowledge financial support from the Agencia Estatal de Investigación of the Ministerio de Ciencia, Innovación y Universidades and the European FEDER/ERF funds through projects AYA2015-69350-C3-2-P, ESP2016-80435-C2-1-R, AYA2016-79425-C3-1/2/3-P, ESP2017-87676-C5-1-R, and the Centre of Excellence "Severo Ochoa" and "María de Maeztu" awards to the Instituto de Astrofísica de Canarias (SEV-2015-0548), Instituto de Astrofísica de Andalucía (SEV-2017-0709), and Centro de Astrobiología (MDM-2017-0737), and the "Generalitat de Catalunya/CERCA programme".

References

Allart, R., Bourrier, V., Lovis, C., et al. 2018, Science, 362, 1384
Alonso-Floriano, F. J., Morales, J. C., Caballero, J. A., et al. 2015, A&A, 577, A128
Alonso-Floriano, F. J., Snellen, I. A. G., Czesla, S., et al. 2019, A&A, 629, A110
Andretta, V., & Giampapa, M. S. 1995, ApJ, 439, 405
Andretta, V., Giampapa, M. S., Covino, E., Reiners, A., & Beeck, B. 2017, ApJ, 839, 97
Andretta, V., & Jones, H. P. 1997, ApJ, 489, 375
Avrett, E. H., Fontenla, J. M., & Loeser, R. 1994, IAU Symp., 154, 35
Baroch, D., Morales, J. C., Ribas, I., et al. 2018, A&A, 619, A32
Caballero, J. A., Cortés-Contreras, M., Alonso-Floriano, F. J., et al. 2016, in 19th Cambridge Workshop on Cool Stars, Stellar Systems, and the Sun (CS19), 148
Cauley, P. W., & Johns-Krull, C. M. 2014, ApJ, 797, 112
Dupree, A. K., Brickhouse, N. S., Smith, G. H., & Strader, J. 2005, ApJ, 625, L131
Dupree, A. K., Brickhouse, N. S., Cranmer, S. R., et al. 2014, ApJ, 789, 27
Dupree, A., Brickhouse, N., Irwin, J., Kurucz, R., & Newton, E. 2018, in Cambridge Workshop on Cool Stars, Stellar Systems, and the Sun, Cambridge Workshop on Cool Stars, Stellar Systems, and the Sun, 87
Edwards, S., Fischer, W., Hillenbrand, L., & Kwan, J. 2006, ApJ, 646, 319
Fuhrmeister, B., Liefke, C., Schmitt, J. H. M. M., & Reiners, A. 2008, A&A, 487, 293
Fuhrmeister, B., Lalitha, S., Poppenhaeger, K., et al. 2011, A&A, 534, A133
Fuhrmeister, B., Czesla, S., Schmitt, J. H. M. M., et al. 2018, A&A, 615, A14
Fuhrmeister, B., Czesla, S., Schmitt, J. H. M. M., et al. 2019, A&A, 623, A24
Garcia-Piquer, A., Morales, J. C., Ribas, I., et al. 2017, A&A, 604, A87
Gomes da Silva, J., Santos, N. C., Bonfils, X., et al. 2011, A&A, 534, A30
Gordon, I. E., Rothman, L. S., Hill, C., et al. 2017, J. Quant. Spectr. Rad. Transf., 203, 3
Hauschildt, P. H., Allard, F., & Baron, E. 1999, ApJ, 512, 377
Hawley, S. L., Allred, J. C., Johns-Krull, C. M., et al. 2003, ApJ, 597, 535
Hilton, E. J., West, A. A., Hawley, S. L., & Kowalski, A. F. 2010, AJ, 140, 1402
Houdebine, E. R., Stempels, H. C., & Oliveira, J. H. 2009, MNRAS, 400, 238
Husser, T.-O., Wende-von Berg, S., Dreizler, S., et al. 2013, A&A, 553, A6
Jeffers, S. V., Schöfer, P., Lamert, A., et al. 2018, A&A, 614, A76
Kausch, W., Noll, S., Smette, A., et al. 2015, A&A, 576, A78
Kobanov, N., Chelpanov, A., & Pulyaev, V. 2018, J. Atmos. Sol. Terr. Phys., 173, 50
Linsky, J. L., Neff, J. E., Brown, A., et al. 1989, A&A, 211, 173
Livingston, W., White, O. R., Wallace, L., & Harvey, J. 2010, Mem. Soc. Astron. It., 81, 643
Mamajek, E. E., Bartlett, J. L., Seifahrt, A., et al. 2013, AJ, 146, 154
Mansfield, M., Bean, J. L., Oklopčić, A., et al. 2018, ApJ, 868, L34
Martin, J., Fuhrmeister, B., Mittag, M., et al. 2017, A&A, 605, A113
Mittag, M., Hempelmann, A., Schmitt, J. H. M. M., et al. 2017, A&A, 607, A87
Mohanty, S., & Basri, G. 2003, ApJ, 583, 451
Nagel, E., Czesla, S., Schmitt, J. H. M. M., et al. 2019, A&A, 622, A153
Newton, E. R., Irwin, J., Charbonneau, D., et al. 2017, ApJ, 834, 85
Nortmann, L., Pallé, E., Salz, M., et al. 2018, Science, 362, 1388
Oliva, E., Origlia, L., Scuderi, S., et al. 2015, A&A, 581, A47
Orozco Suárez, D., Asensio Ramos, A., & Trujillo Bueno, J. 2014, A&A, 566, A46
Passegger, V. M., Reiners, A., Jeffers, S. V., et al. 2018, A&A, 615, A6
Passegger, V. M., Schweitzer, A., Shulyak, D., et al. 2019, A&A, 627, A161
Pizzolato, N., Maggio, A., Micela, G., Sciortino, S., & Ventura, P. 2003, A&A, 397, 147
Quirrenbach, A., Amado, P. J., Ribas, I., et al. 2018, Proc. SPIE Conf. Ser. 10702, 107020W
Rauscher, E., & Marcy, G. W. 2006, PASP, 118, 617
Reiners, A., Zechmeister, M., Caballero, J. A., et al. 2018, A&A, 612, A49
Robertson, P., Bender, C., Mahadevan, S., Roy, A., & Ramsey, L. W. 2016, ApJ, 832, 112
Rothman, L. S., Gordon, I. E., Babikov, Y., et al. 2013, J. Quant. Spectr. Rad. Transf., 130, 4
Salz, M., Czesla, S., Schneider, P. C., et al. 2018, A&A, 620, A97
Sanz-Forcada, J., & Dupree, A. K. 2008, A&A, 488, 715
Schmidt, S. J., Kowalski, A. F., Hawley, S. L., et al. 2012, ApJ, 745, 14
Schöfer, P., Jeffers, S. V., Reiners, A., et al. 2019, A&A, 623, A44
Schweitzer, A., Passegger, V. M., Cifuentes, C., et al. 2019, A&A, 625, A68
Smette, A., Sana, H., Noll, S., et al. 2015, A&A, 576, A77
Smith, G. H. 2016, PASA, 33, e057
Spake, J. J., Sing, D. K., Evans, T. M., et al. 2018, Nature, 557, 68
Stauffer, J. R., & Hartmann, L. W. 1986, ApJS, 61, 531
Takeda, Y., & Takada-Hidai, M. 2011, PASJ, 63, 547
Vaughan, Jr., A. H., & Zirin, H. 1968, ApJ, 152, 123
Voges, W., Aschenbach, B., Boller, T., et al. 1999, A&A, 349, 389
West, A. A., Morgan, D. P., Bochanski, J. J., et al. 2011, AJ, 141, 97
Zarro, D. M., & Zirin, H. 1986, ApJ, 304, 365
Zechmeister, M., Anglada-Escudé, G., & Reiners, A. 2014, A&A, 561, A59
Zechmeister, M., Reiners, A., Amado, P. J., et al. 2018, A&A, 609, A12
Zirin, H. 1982, ApJ, 260, 655

Appendix A: Examples of other chromospheric lines in the spectra

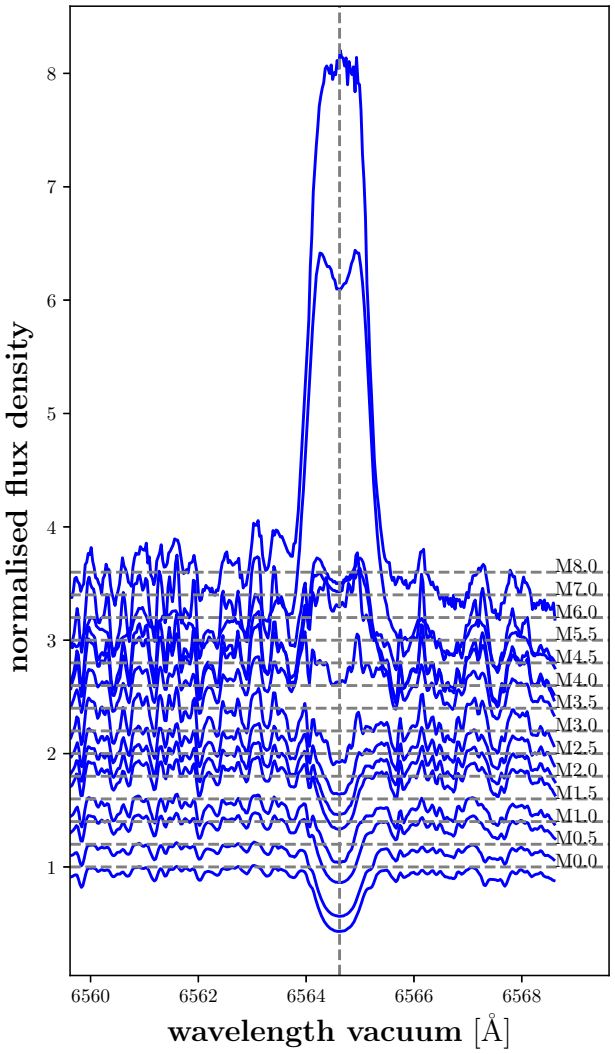

Fig. A.1. Spectral-type series for region around Hα. Each normalised spectrum (blue line) is offset by 0.2 in flux density for clarity purposes. The continuum for each spectrum is marked with a dashed grey line. The position of the line centre is marked with a grey dashed vertical line. While early M dwarfs are typically inactive (showing Hα in absorption), mid- to late-type M dwarfs are typically active, with very variable Hα emission. The shown stars are (same as in Fig. 2): M0.0 V: J03463+262/HD 23453. M0.5 V: J02222+478/BD+47 612. M1.0 V: J00051+457/GJ 2. M1.5 V: J02123+035/BD+02 348. M2.0 V: J01013+613/GJ 47. M2.5 V: J00389+306/Wolf 1056. M3.0 V: J02015+637/G 244-047. M3.5 V: J12479+097/Wolf 437. M4.0 V: J01339-176/LP 768-113. M4.5 V: J01125-169/YZ Cet. M5.5 V: J00067-075/GJ 1002. M6.0 V: J14321+081/LP 560-035 M7.0 V: J02530+168/Teegarden's star. M8.0 V: J19169+051S/vB10.

Here we provide some representative examples of the other chromospheric lines used as a comparison for the He I IR line measurements. In Fig. A.1 we show the same spectral-type series as in Fig. 2 but for the wavelength region around Hα. In Figs. A.2 and A.3 we show the same for the bluest Ca II IRT and the He I D_3 line. The slope in the continuum for the He I D_3 line is caused by the vicinity of the Na I D lines, which have broad absorption wings.

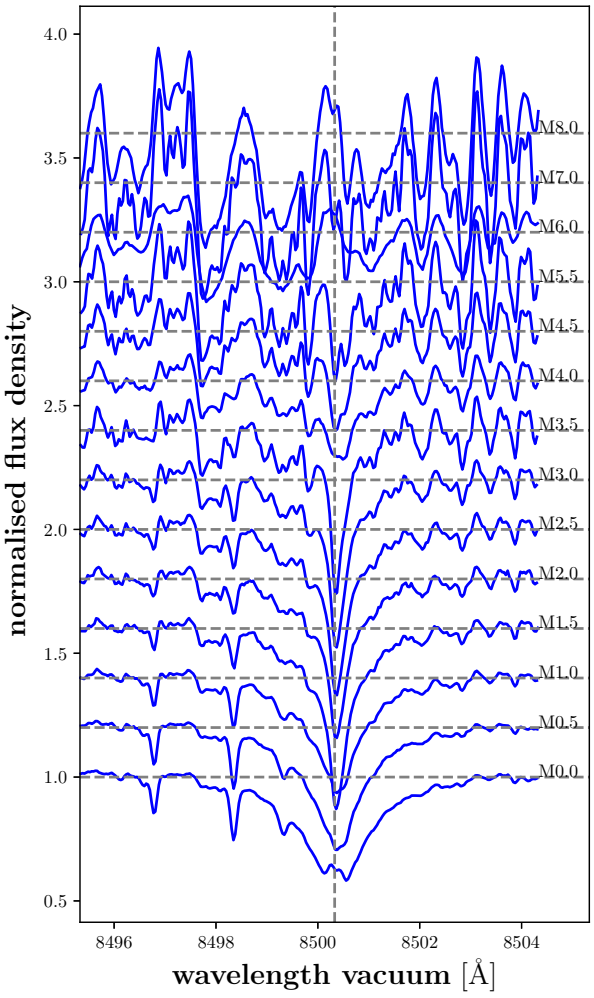

Fig. A.2. Spectral-type series for region around bluest line of Ca II IRT. Each normalised spectrum (blue lines) is offset by 0.2 in flux density for clarity purposes. The background for each spectrum is marked with a dashed grey line. The position of the line centre is marked with a grey dashed vertical line. The shown stars are the same as in Figs. 2 and A.1.

We want to illustrate our search for other He I lines in the optical by using as an example the very active M4.5 V star J07446+035/YZ CMi. We show in Fig. A.4, the He I D_3 line which is in emission. The slight asymmetry to the red side is caused by another component of the line. On the other hand, the He I line at 6678 Å is, at best, ambiguous, but most likely hidden in the molecular lines.

This is a typical example of a mid M dwarf, where Hα and He I D_3 are emission lines, but other He I lines in the optical are not seen during quiescent state. For more early-type M dwarfs (which are usually inactive) the He I D_3 is absent as well.

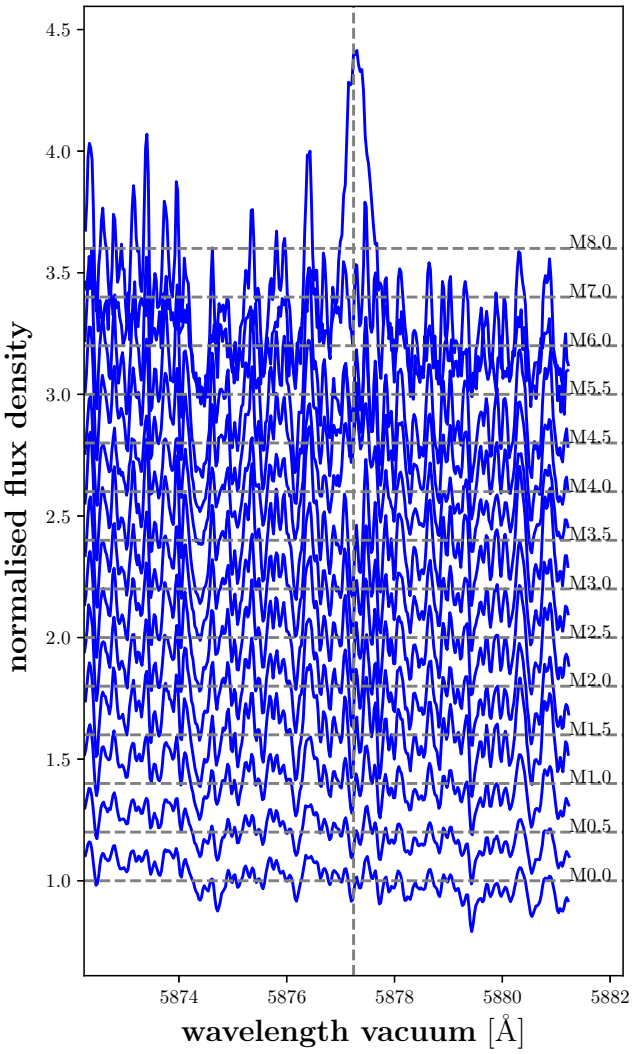

Fig. A.3. Spectral-type series for region around He I D_3 line. Each normalised spectrum (blue line) is offset by 0.2 in flux density for clarity purposes. The background for each spectrum is marked with a dashed grey line. The position of the line centre is marked with a grey dashed vertical line. The stars shown are the same as in Figs. 2 and A.1.

Appendix B: X-ray luminosity compared to effective temperature

For the purposes of comparison, we also show in Fig. B.1 the distribution of the L_X/L_{bol} values as a function of the effective temperature T_{eff} including upper limits in the L_X/L_{bol} measurements.

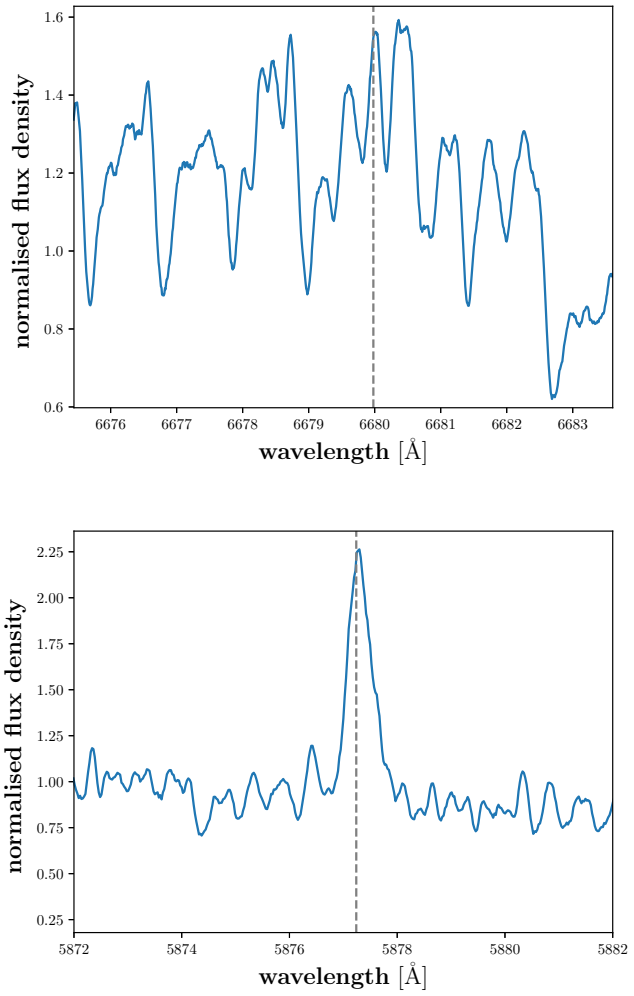

Fig. A.4. Examples of spectral regions around He I line at 6679 Å (*top*) and He I D_3 line at 5877 Å (*bottom*) for J07446+035/YZ CMi. Positions of the two lines are marked with grey dashed vertical lines.

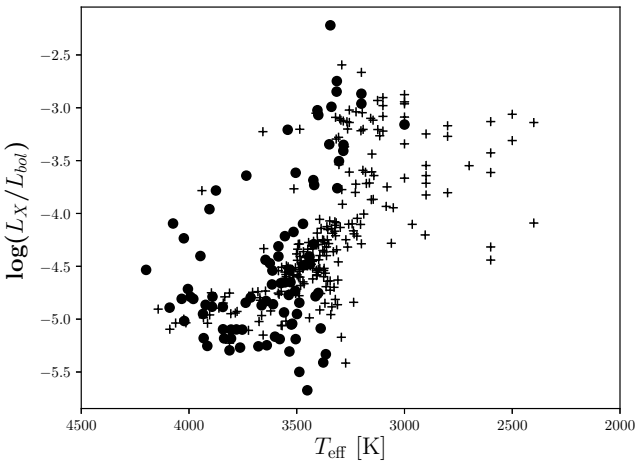

Fig. B.1. Distribution of L_X/L_{bol} as function of T_{eff}. Black dots denote L_X/L_{bol} measurements for our valid sample. Black crosses denote upper limits for L_X/L_{bol} for the whole sample, including stars which do not qualify for the valid sample.

Appendix C: Spectral series of the He I IR line

Here we show the development of the He I IR line with spectral type. In Figs. C.1 and C.2 we show the He I IR line for M0.5 V to M7.0 V stars. While the Si I line has a tendency to diminish towards late spectral types, the absorption features at 10 832 Å gain in depth. The He I IR line also diminishes towards late spectral types and develops some asymmetry with more flux in the red side from spectral type M3.5 V on, which apparently belongs to a strengthening feature that is unidentified, molecular perhaps, and also persistent for the very late types where the He I IR line vanishes.

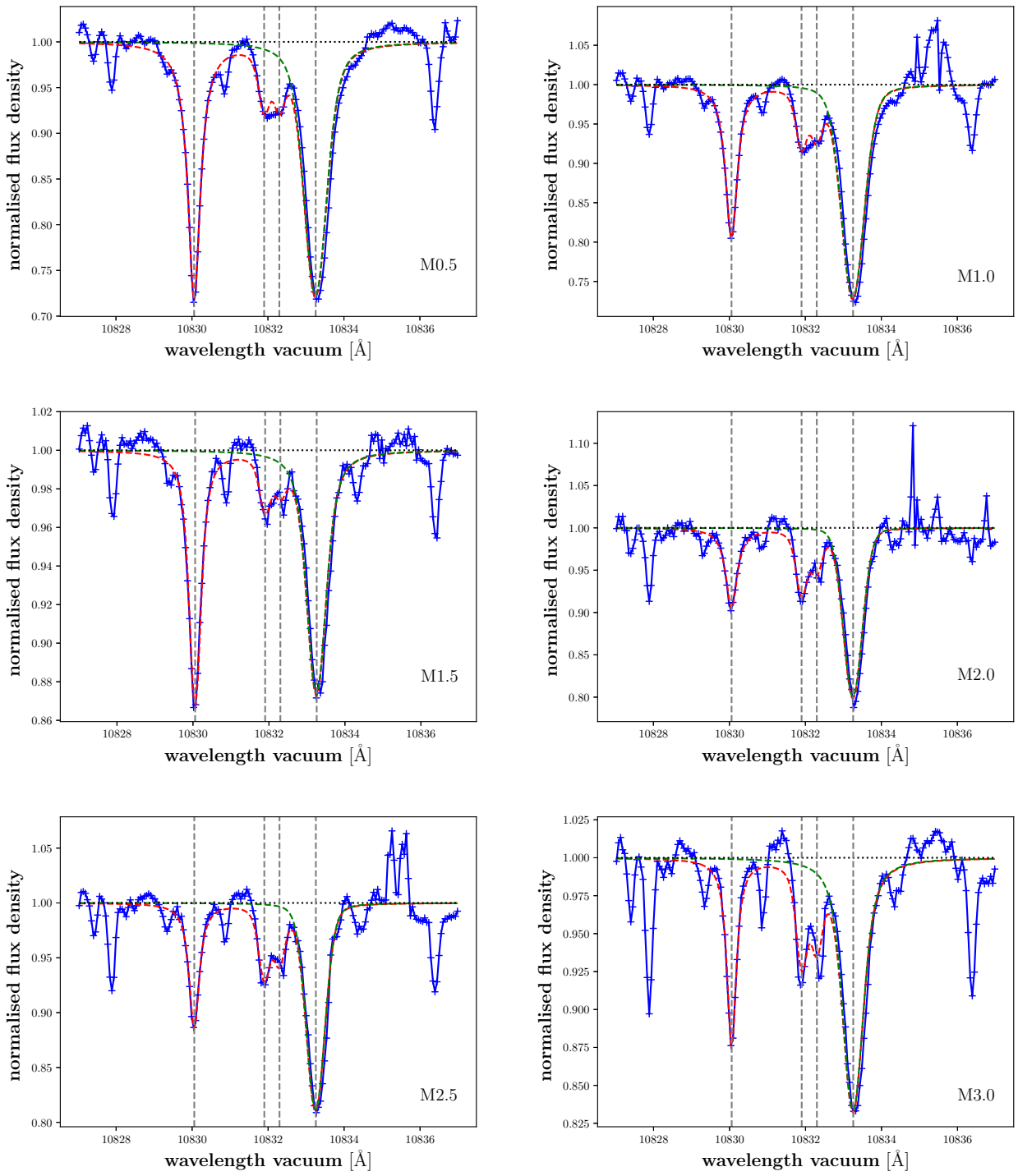

Fig. C.1. Examples for He I IR line and neighbouring spectral region as it changes along with a spectral type similar to Fig. 2 while also displaying Voigt fits. The observed spectrum is denoted in blue, fit in red, and fit component of the He I IR line in green (dashed). Vertical grey dashed lines mark the position of lines considered in the fit (Si I line at 10 830.057 Å, He I IR line at 10 833.25 Å, two unidentified lines at 10 831.9 and 10 832.3 Å.) *Top left*: M0.5 V star J02222+478/BD+47 612. *Top right*: M1.0 V star J00051+457/GJ 2. *Middle left*: M1.5 V star J02123+035/BD+02 348. *Middle right*: M2.0 V star J01013+613/GJ 47. *Bottom left*: M2.5 V star J00389+306/Wolf 1056. *Bottom right*: M3.0 V star J02015+637/G 244-047.

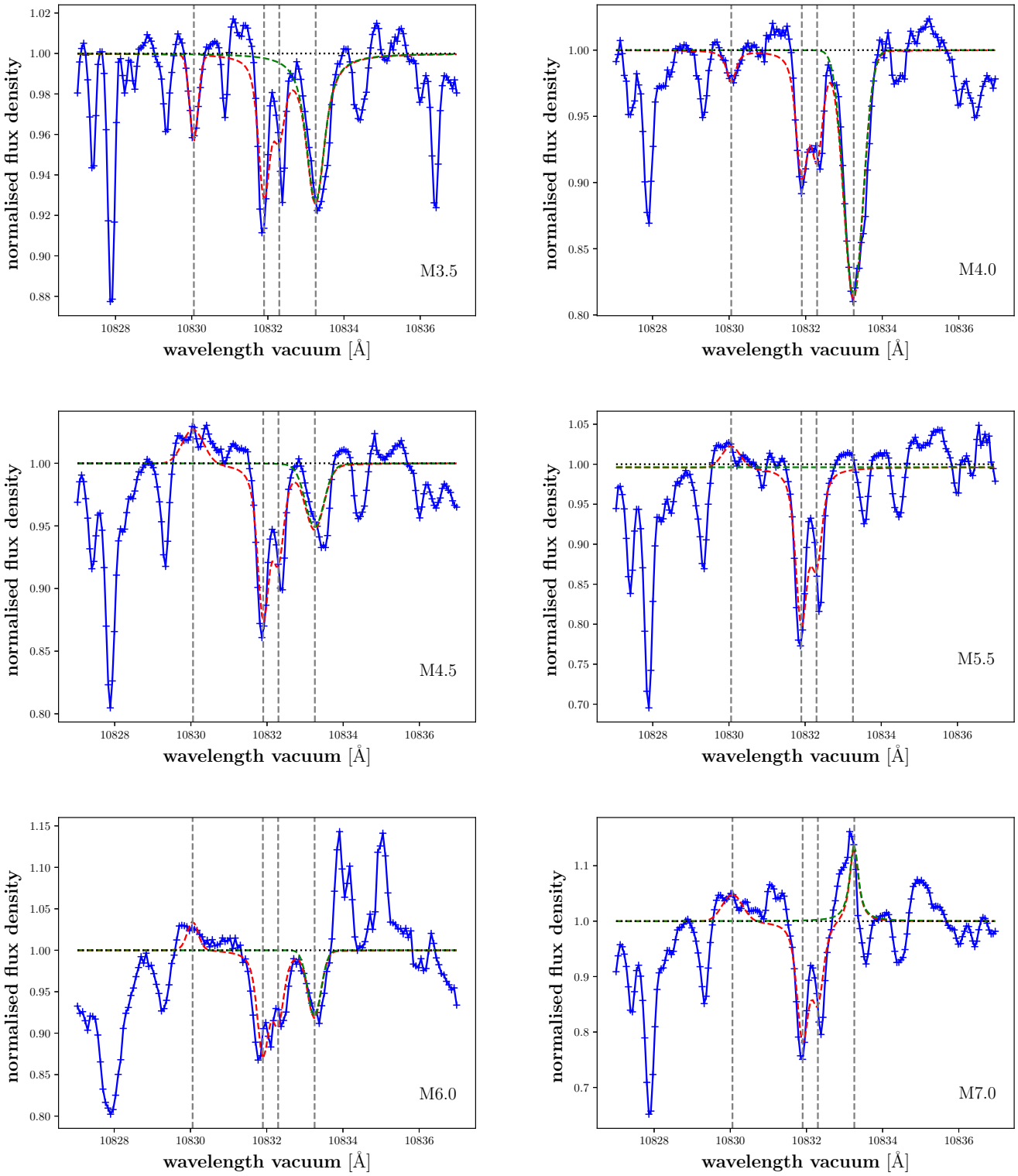

Fig. C.2. Same as Fig. C.1, but for later spectral types. *Top left*: M3.5 V star J12479+097/Wolf 437. *Top right*: M4.0 V star J01339-176/LP 768-113. *Middle left*: M4.5 V star J01125-169/YZ Cet. *Middle right*: M5. V5 star J00067-075/GJ 1002 star. *Bottom left*: M6.0 V star J14321+081/LP 560-035 showing some emission artefacts red-wards of the He I line as well. *Bottom right*: M7 V star J02530+168/Teegarden's star.